Chapter 31
Laser Structuring for Biomedical Applications

Gerda Buchberger, Martina Muck, Cristina Plamadeala, and Johannes Heitz

Abstract Laser structuring enables modification of sample topography, surface chemistry, and/or physical properties of materials. Examples of these processes are ripple, nap or wall formation, surface oxidation, induction of polymerization reactions, or changes in crystallinity or contact angle. These – most of the time – interrelated modifications are exploited widely for biomedical applications. They range from cell-repellent surfaces for easy-to-replace cardiac pacemakers, control of cell proliferation required in regenerative medicine, to increased cell adhesion for cell arrays. Furthermore, ns-laser-induced nanoripples were used for formation of gold nanowires for future surface plasmon resonance sensors directly integrated into biotechnological devices. Additive nano- and microscale manufacturing by two-photon polymerization allows for considerable progress in cell scaffold formation, paving the path for in vitro–grown organs, bones, and cartilages. The very same fs-laser-based technique was also used for biomimetic microneedles with enhanced liquid spreading on their surface. Microneedles are promising candidates for low-cost, high-throughput drug delivery and vaccination applicable even by nonmedically trained personnel. Microfluidic systems fabricated by fs-lasers have enabled progress in 3D microscopy of single cells and in studies on thrombocyte activation with the help of nanoanchors. Explicating the abovementioned and further biomedical applications, the authors put special focus on the achieved limits pointing out what scientists have accomplished so far in their pursuit of extreme scales.

Keywords Microstructures · Nanostructures · Microneedles · Cell scaffolds · Repellent · Adhesion · Activation of cells

G. Buchberger (✉) · M. Muck · C. Plamadeala · J. Heitz (✉)
Institute of Applied Physics, Johannes Kepler University (JKU) Linz, Linz, Austria
e-mail: gerda.buchberger@jku.at; martina.muck@jku.at; cristina.plamadeala@jku.at; johannes.heitz@jku.at

1105

Abbreviations

AFM	Atomic force microscopy
ALD	Atomic layer deposition
ANN	Artificial neural networks
AOM	Acousto-optical modulator
BG	Bioactive glass
CAD	Computer-aided design
CCD	Charge-coupled device
CHO	Chinese hamster ovary
CNN	Convolutional neural networks
DCM	Dichloromethane
DCP	Dichloropentane
DIMP	Diisopropyl methylphosphonate
DLIP	Direct laser interference patterning
DLW	Direct laser writing
DLW SM	Direct laser writing for subtractive manufacturing
DMMP	Dimethyl methylphosphonate
EBL	Electron beam lithography
ECM	Extracellular matrix
ECSA	Electrochemical surface area
ELI	Extra low interstitial
EUV	Extreme ultraviolet
FEA	Finite element analysis
FEP	Fluorinated ethylene propylene
FLICE	Femtosecond laser irradiation followed by chemical etching
FN	Fibronectin
HA	Hydroxyapatite
HEK	Human embryonic kidney
HMEC	Human microvascular endothelial cell
HUVEC	Human umbilical vein endothelial cell
IR	Infrared
LC	Laser cladding
LIFT	Laser-induced forward transfer
LIL	Laser interference lithography
LIPSS	Laser-induced periodic surface structures
MAPLE	Matrix-assisted pulsed laser evaporation
MIFE	Microelectrode ion flux estimation
MN	Microneedle
MPL	Multiphoton lithography
MSC	Mesenchymal stem cells
NBDS	Nonbulbar dermal sheath
NOA 61	Norland Optical Adhesive 61
OCN	Osteocalcin
OLN-93	Oligodendroglia cell line
OND	Oligonucleotide
OPA	One-photon absorption
PE	Poly(ethylene)
PEG-DA	Poly(ethylene glycol diacrylate)
PET	Poly(ethylene terephthalate)
PETA	Pentaerythritol tetraacrylate
PLA	Poly(lactive) acid
PLD	Pulsed laser deposition

PLGA   Poly(lactive-co-glycolic) acid
PMMA   Poly(methyl methacrylate)
PPy   Poly(pyrrole)
PS   Poly(styrene)
PSF   Point spread function
PU   Poly(urethane)
RIU   Refractive index units
SAW   Surface acoustic wave
SEM   Scanning electron microscopy
SERS   Surface-enhanced Raman scattering
SGC   Spinal ganglion cells
SH   Sodium hyaluronate
SLIPS   Slippery liquid-infused porous surfaces
SLS   Selective laser sintering
SPP   Surface plasmon polariton
STED   Stimulated emission depletion
STL   Stereolithography
TE   Tissue engineering
TPA   Two-photon absorption
TPL   Two-photon lithography
TPP or 2PP Two-photon polymerization
TRL   Technology readiness level
UV   Ultraviolet
VN   Vitronectin
WGM   Whispering gallery mode
WP   Waveplate

1   Introduction: Overview on Laser Structuring

Section 1 provides a short overview on laser structuring methods commonly used in biomedical applications. Properties like size, shape, and pattern of laser structures as well as the irradiated material type determine the potential for a specific biomedical application. Laser structures come in two different forms: self-organized (Sect. 1.1) or directly written (Sect. 1.2), and can form on various material classes like metals, polymers, and dielectrics. Lasers have also proven to be able to chemically modify surfaces by processes like direct surface irradiation and deposition of thin films. Prominent examples for indirect surface modification with lasers are pulsed laser deposition (PLD) and matrix-assisted pulsed laser evaporation (MAPLE) (Sect. 1.3).

1.1   Self-Organization

Usually, irradiating materials with lasers results in a morphological change of the processed surface, which either leads to self-organized laser-induced structures or direct laser-inscribed structures [1]. For self-organized structures, the laser beam
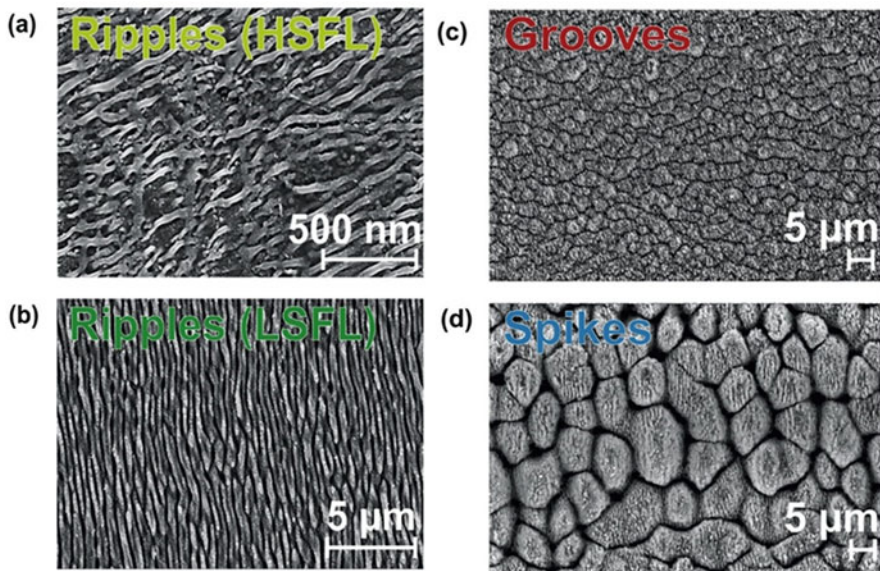
Fig. 31.1 SEM images of LIPSS with (**a**) high and (**b**) low spatial frequency, (**c**) microgrooves, and (**d**) micro-sized spikes with superimposed nanoripples. (Reprinted from Hermens et al. [11], Copyright (2017), with permission from Elsevier)

irradiates the surface in a spot or another scanning geometry, leading to the formation of (quasi-)periodic surface morphologies. An overview of self-organized structures is shown in the scanning electron microscope (SEM) images of Fig. 31.1. These structures can be found on the micrometer as well as on the nanometer range. Microstructures are usually known as grooves and spikes (Fig. 31.1c, d) and nanostructures as laser-induced periodic surface structures (LIPSS) or ripples (Fig. 31.1a, b) [2–4]. The irradiating laser commonly has a Gaussian intensity spatial profile and a spatially homogeneous linear polarization. However, several attempts showed that the complexity of self-organized structures can be increased if inhomogeneous beam profiles and nonlinear laser polarizations are used [5–8]. As an example, it was reported that circularly polarized ultrafast laser pulses can be used to create micro-metric triangular surface structures [9, 10]. Self-organized structures have been reported on various material classes such as metals [1, 11, 12], polymers [13–16], and others [17–19]; however, the types of structures that can form depend on the properties of the irradiated material.

To control the outcome of the structure morphology, a proper selection of the laser processing parameters is required. This includes choosing proper combinations of parameters such as peak fluence Φ_0 and effective number of laser pulses N. For various biomedical applications, it is also necessary that laser-induced structures show a pronounced morphological complexity, which will be discussed in further detail in Sect. 2.1. Only a few approaches on creating complex morphological

hierarchies of micro- and nano-metric structures were reported. These include surface irradiation with ultrafast laser pulses in reactive atmosphere [20, 21] or multistep surface processing, which combines both self-organized and directly written laser structures [22, 23]. The process of surface patterning by laser irradiation and formation of laser structures is discussed in detail in Chaps. 12, 13, and 28 of Bäuerle [24]. Self-organized laser-induced structures have been featured on various materials for biomedical applications [25–30], especially in the field of cell behavior control, which will be discussed in Sects. 2.1 and 2.2. An overview of the formation of laser-induced self-organized structures, especially of the ones mimicking biological surfaces, is reported in Stratakis et al. [31].

To get an insight on the precision limit and reproducibility of laser-based nanostructuring, the reader is encouraged to check Chap. 8 of this book. Chapter 23 describes in detail the formation and the wide range of applications of LIPSS. Complex designs of micro- and nanostructures can additionally be achieved by interference pattering methods such as laser interference lithography (LIL) or direct laser interference patterning (DLIP). These methods and their applications, where some of them are of biomedical nature, are described in Chap. 26.

1.2 Direct Writing

Direct laser writing (DLW) for biomedical applications includes subtractive as well as additive laser processing techniques. A special form of direct laser writing is two-photon polymerization (TPP or 2PP), also known as two-photon lithography (TPL or 2PL). TPP is a three-dimensional (3D) additive micro- and nanofabrication technique [32] which is based on the process of simultaneous absorption of two photons (two-photon absorption, TPA) [33]. In TPA, a molecule absorbs one photon and is excited from its ground state to a virtual state. The lifetime of the virtual state is in the order of femtoseconds (10^{-15} s). If within this lifetime the molecule absorbs another photon, the molecule reaches an excited state. If not, the virtual state collapses to the ground state. As TPA depends on the simultaneous absorption of two photons, the probability of the process depends on the second power of the light intensity, which makes the process highly localized. Hence, the polymerization can be confined three-dimensionally, and feature sizes under 200 nm can be obtained [33].

Practically, the simultaneous absorption of two photons and sub-diffraction structures are achieved by setups containing an ultrashort-pulsed laser system (which ensures the absorption of two photons within the lifetime of the virtual state), focusing optics, and sample positioning and/or beam deflection elements (such as linear stages, piezo-systems, and galvanometer scanners). For direct writing of complex 3D structures, a user-defined 3D model is created in a computer-aided design (CAD) software, which is exported into a stereolithography (STL) file. The STL file describes the surface of the 3D object and communicates this information to the elements responsible to translate the laser beam focus relative
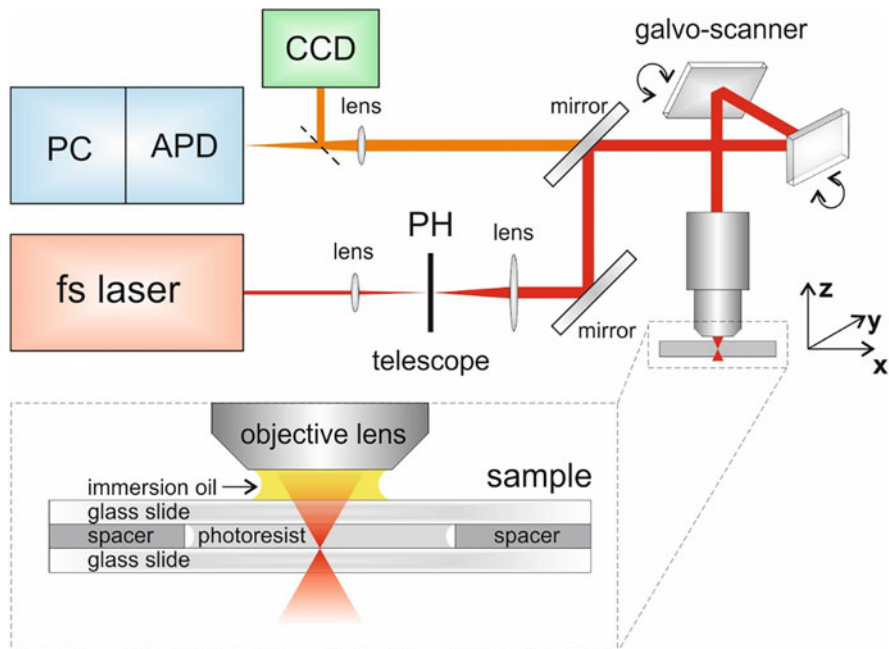
Fig. 31.2 Principle setup for TPP microfabrication of 3D structures. A fs-laser beam is expanded by a telescope and directed into a *xy* galvanometer scanner. The beam is later focused by a high numerical aperture (NA) objective lens into the sample, which is mounted on a 3D piezo-stage. Abbreviations: personal computer (PC), avalanche photodiode (APD), charge-coupled device (CCD), pinhole (PH)

to the substrate and the photoresist [32]. More simple structures can be achieved by any computer controlling the precise movement of the *x, y, z*-stages (or even by moving the stages manually using a joystick). To obtain even smaller features sizes (under 100 nm), stimulated emission depletion (STED) lithography can be employed, where a second laser is used to inhibit the polymerization in the outer rim of the focal point [34]. A principle TPP setup is shown in Fig. 31.2.

Materials used in TPP have to possess the following properties [32]: (1) refractive index close to 1.5, to avoid or minimize aberrations when focusing the laser beam into the resist; (2) transparency for the laser beam wavelength, to avoid one-photon absorption (OPA) processes; (3) fast curing with minimal shrinkage; and (4) good adhesion to the substrate and mechanical strength [35]. Commercially available epoxy- (SU-8 series) and acrylic-based (OrmoComp® series) photoresists, as well as custom-tailored ones, are used for a wide range of applications in photonics, micro-electronics, and micro-mechanics [36], as well as in biomedicine. For the latter one, material selection is even more rigorous, as in some applications not only biocompatibility [37] but also biodegradability is required [38].
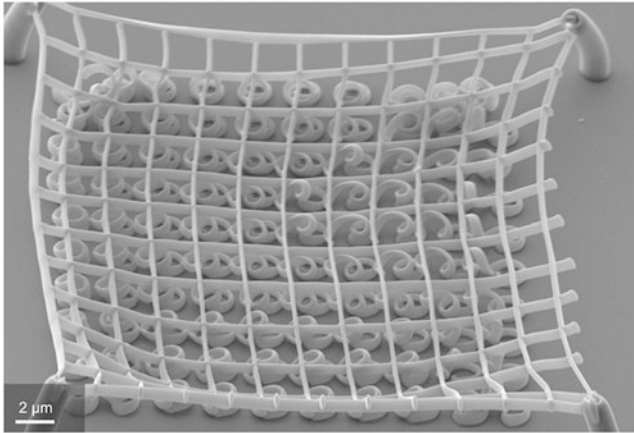
Fig. 31.3 Microstructures of variable geometries written with an acrylate-based photoresist by means of TPP. (By courtesy of Richard Wollhofen, Johannes Kepler University Linz, Austria)

The TPP technique allows the fabrication of micro- and nanostructures of variable geometries in two or three dimensions, which is demonstrated exemplarily in Fig. 31.3.

Besides additive laser processing (such as TPP), subtractive laser processing techniques (also generally known under the term of "laser ablation") are also relevant in biomedical applications. Direct laser writing techniques for subtractive manufacturing (DLW SM) range from material removal and surface modifications [39–41] to laser drilling [42], cutting [43], and welding [44]. Generally, a setup used for these applications contains a laser beam that is shaped by optical elements and focused onto a sample that is mounted onto a translation or rotation stage. DLW SM is used to process polymers [45], zirconia-based ceramics [39], and metals [41], for example, for tissue engineering and biosensing applications.

To get an insight into biological applications of TPP and DLW SM, the reader is encouraged to check Sects. 2.3 and 2.5. The reader is also advised to read the part on subtractive and additive structuring methods in Chap. 8 of this book. Chapter 22 describes multiphoton 3D lithography, which can be used in various fields such as photonics and microfluidics.

1.3 Non-topographical Modifications

Surface modification is often accompanied with the goal of maintaining the bulk material properties. This can be achieved by physically or chemically altering the existing surface or completely changing it by covering it with thin films of a different material [46]. Various thin films on metal alloys such as hydroxyapatite (HA), glass ceramics, and glasses have been employed to change the surface for

more biocompatibility. Modifying the surface chemistry plays a key role in the adsorption of proteins such as fibronectin (FN) and vitronectin (VN), which further control cell adhesion. Pulsed laser deposition (PLD) [47] and matrix-assisted pulsed laser evaporation (MAPLE) [48] are examples for laser-assisted cell-biomaterial interaction control (both techniques are described in Chap. 22 of Bäuerle [24]). PLD is often used for deposition of hydroxyapatite or bioactive glass (BG) layers on metallic and polymeric implant surfaces to improve biofunctionality [49–51]. Koch et al. [52] produced bioglass thin films on polished titanium samples by PLD. MAPLE is an extension of the PLD process for growing thin films consisting of polymeric materials, which allows deposition of heat-sensitive molecules with minimal degradation [53, 54]. The possibility to deposit fibronectin molecules with MAPLE, which facilitate the attachment of human osteoprogenitor cells, was reported for silicon substrates [55]. Lactoferrin, an iron-binding glycoprotein, plays an important role in host defense against viral and microbial infections. Constantinescu et al. [56] studied lactoferrin layers produced by MAPLE on different materials to evaluate their biocompatibility and revealed that MAPLE is an excellent process for improved drug delivery due to the possibility of coating drugs with a thin film, thus inhibiting unwanted reaction with a solvent. Additionally, it was reported that biocompatible polymers such as poly(lactive-co-glycolic) acid (PLGA) can be coated by MAPLE for controlled drug delivery [57]. Dinca et al. [58] reported that MAPLE is suitable for obtaining active polymeric-enzymatic interfaces as hybrid or layered coatings for detecting toxic vapors such as dimethyl methylphosphonate (DMMP) and diisopropyl methylphosphonate (DIMP). Electrical stimuli have proven to be of great importance for tissue engineering, and Paun et al. [59] used a MAPLE approach to produce conductive poly(pyrrole) (PPy)-based composite layers to promote new bone formation. These composite layers consist of conductive PPy nanograins in a biocompatible polymeric matrix, such as PLGA or polyurethane (PU).

Chemical modification of surfaces by laser treatment has been used extensively due to its potential of achieving corrosion resistance, self-cleaning, and anti-fouling, which is discussed in detail in Chap. 24 of this book. Corrosion resistance is achieved by surface oxides, which can be formed by laser treatment [24, 60–62] or can be induced by chemical treatments such as anodic oxidation [63, 64]. Laser irradiation can cause bond breaking in polymers, leading to the formation of radicals and subsequent reaction with the surrounding atmosphere. This process is of great importance for biological processes such as cell adhesion [24, 65]. Furthermore, the surface wettability, which is essential for cell growth, can also be modified by laser irradiation [66, 67]. Excimer laser irradiation of poly(ethylene terephthalate) (PET), for example, modifies the surface chemistry of the polymer [68–70] as well as its wettability [68, 70] depending on the applied fluence. Heitz et al. [71] have shown that laser processing of titanium alloy surfaces resulted in a hydrophilic behavior, which changed steadily to a hydrophobic behavior after a few weeks. Subsequent electrochemical anodization of hydrophobic surfaces resulted again in a hydrophilic surface, which also changed back to hydrophobicity after a couple of weeks. The reason for these effects is still an ongoing research topic, but it is believed to result
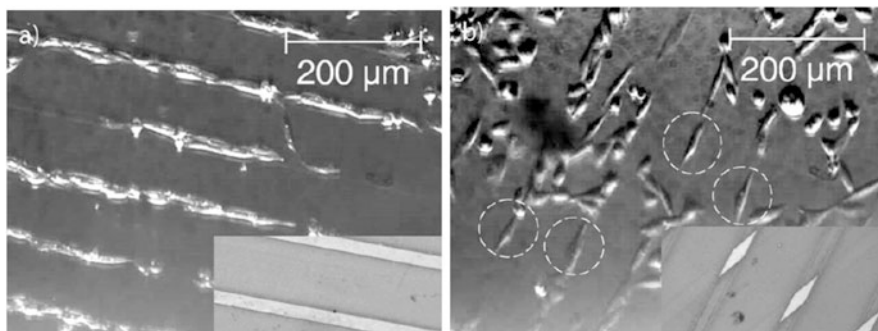
Fig. 31.4 Optical microscopy images of CHO cells seeded on patterned FEP samples: (**a**) lines and (**b**) rhombs (images taken on living cells). Insets are optical microscopy images of the FEP structures before cell seeding (in the same scale). The dashed circles in (**b**) indicate exemplary cells with a shape directly affected by the wettable islands. (Reprinted from Yakunin et al. [73], © 2011 Wiley Periodicals, Inc.)

from chemical bond breaking and reaction with the ambient atmosphere. Ranella et al. [72] investigated how wetting affects fibroblast growth on silicon, concluding that fibroblastic growth is reduced for hydrophobic surfaces.

The combination of the techniques described in this section (i.e., PLD, MAPLE, chemical modification) with laser patterning allows the fabrication of functional micro- and nanostructures. This is illustrated exemplarily in Fig. 31.4, which shows isolated Chinese hamster ovary (CHO) cells grown on a laser-structured photomodified fluorinated ethylene propylene (FEP) surface [73].

2 Biomedical Applications

Section 2 gives an overview on how laser irradiation of different surfaces can be used for biomedical applications. Cell behavior control by physical and chemical modification of surfaces has proven to be of great importance for medical implants and tissue engineering (Sects. 2.1 and 2.2), and 3D support systems such as cell arrays and scaffolds have been shown to create a viable cell environment that replaces the natural surroundings of cells (Sect. 2.3). Microneedles that incorporate directional fluid transport inspired by nature could be employed as minimal-invasive alternatives for commonly used drug delivery systems (Sect. 2.4). Fluidic systems and analysis techniques profit from laser processing, which opens up entirely new possibilities in these fields (Sect. 2.5). Laser structuring is used in the fabrication of biomedical sensors in various ways, for example, in respiratory monitoring or in the detection of cancer cell metabolites, DNA damage, or volatile organic compounds (Sect. 2.6). Section 2.7 gives an introduction on applications where lasers can additionally be used for biomedical purposes, such as bond strengthening and deposition of thin films.

2.1 Micro- and Nanostructures for Adhesion, Alignment, and Activation of Cells

Interactions between cells and surfaces of biomaterials have been proven to be of great importance in the field of biomedicine and tissue engineering [74]. Biomaterials are constituted from a large range of natural and synthetic materials and can be classified into "bio-inert" and "bio-reactive or bioactive". Many studies in the past few years focused on modifying the surface chemistry and morphology to achieve improved biocompatibility and therefore enhance cell attachment, alignment, and proliferation [75–80]. While it was shown that the optimal microroughness for enhancing biocompatibility is strongly cell-type dependent, it is known that an additional roughness in the nm range strongly promotes cell adhesion and proliferation [81, 82]. One reason might be that the structured surfaces with nano-sized features resemble the nanostructures found in the extracellular matrix (ECM) of the cells [83], another that protein adsorption from bodily fluids prior to cell colonization is majorly influenced by physical/chemical properties of the underlying surface [84–88]. Recent studies investigated the influence of nano-metric surface structures on protein adsorption that are relevant for further cell attachment processes, which concluded in the assumption that only features in the size range of surface-bound proteins (~10 nm) affect the adsorption [89–93]. When mammalian cells are grown in vitro, adhesion to the cell culture substrate or to the ECM plays a key role for many processes, like proliferation and differentiation. Cells attach to the surface via focal adhesions, which are integrin-containing, multi-protein structures, that connect the ECM to the cytoskeleton [94].

Many researchers investigated the formation of self-organized structures on polymer foils by irradiation with polarized ultraviolet (UV) laser beams [95–99]. Laser-induced periodic surface structures on polymer films have shown to be beneficial for enhanced adhesion and proliferation of cells as well as for cell alignment. Among them are poly(styrene) (PS) foils, a material widely used in cell culture applications. Rebollar et al. [100] investigated human embryonic kidney cells (HEK-293 cells) and CHO-K1 behavior on LIPSS generated on PS foils by UV irradiation. Both cell types showed alignment on LIPSS with periodicities $\Lambda >$ 270 nm, which is demonstrated in Fig. 31.5 for CHO-K1 cells. It was demonstrated that the cells align along the direction of the ripples and show enhanced adhesion and proliferation compared to unmodified PS foils. However, alignment is highly cell-type dependent and only occurs when the periodicity of the ripples is above a critical value.

However, Schernthaner et al. [101] investigated human microvascular endothelial cells (HMECs) on both micro-metric walls and nano-metric LIPSS fabricated on PET foils and reported that the alignment of HMECs is not influenced by structures with periodicities $\Lambda < 1$ μm, but the proliferation is highly increased by the nano-metric features. Proliferation in endothelial cells is guided by β-catenin, an important transcriptional regulator, which is located within cell-cell contacts in the cell membrane and translocates into the nucleus upon cell activation by proliferative
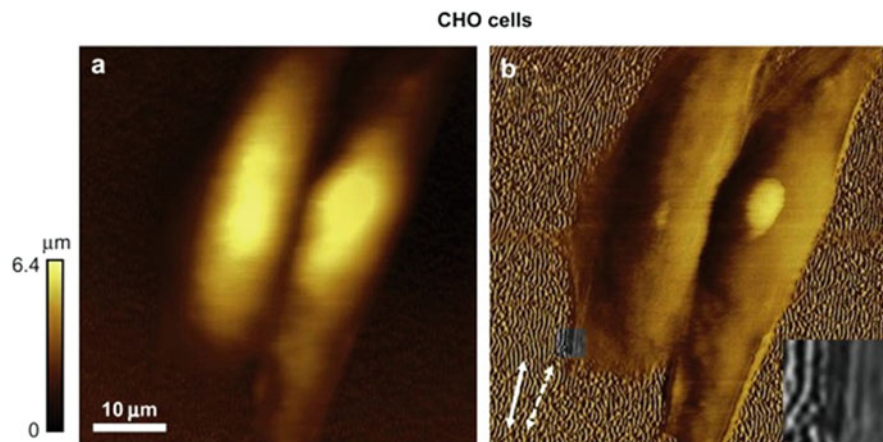
Fig. 31.5 (**a**) Atomic force microscopy (AFM) topographical and (**b**) deflection images of CHO-K1 cells on laser-textured PS foils: The cells align along the ripple direction; in (**b**) the aligned actin filaments of the cells are highlighted in the bottom right corner. (Reprinted from Rebollar et al. [100], Copyright (2008), with permission from Elsevier)

stimuli [102, 103]. This is shown in Fig. 31.6, where HMECs align along the wall-like microstructures, but not on the nano-metric LIPSS, which only enhance cell growth. This effect can also be observed in Fig. 31.7, where a confocal microscope image of vascular progenitor cells was taken on both unstructured and PET surfaces with ripples. The image shows β-catenin located in the interface regions between the cells for the unstructured PET substrate, while β-catenin is extensively found in the nucleus for the surface with ripples.

Additionally, Schernthaner et al. [104] showed that β-catenin activation is guided by enhanced tyrosine phosphorylation involving different types of tyrosine kinases. The type of tyrosine kinase responsible for β-catenin translocation depends on the underlying surface, and this has been shown for HMECs grown on the differently structured PET substrates in the presence of different tyrosine kinase inhibitors.

Even though UV or infrared (IR) laser light is often used to structure material surfaces, extreme ultraviolet (EUV) irradiation has also shown to be able to change the morphology of a treated surface. EUV structures are not as extensively studied as structures fabricated by larger wavelengths due to setup limitations in the past, but are of high interest due to the possibility to create structures that are only a few nanometers large. Reisinger et al. [105] created nano-metric structures with different shapes depending on the peak fluence and the number of applied pulses by EUV irradiation of 50 μm-thick biaxially oriented PET foils (Fig. 31.8). The radiation source was based on a laser-irradiated gas-puff target [106, 107]. But not only was the surface morphology changed by EUV irradiation, also the chemical composition of the surface changed due to photo-induced chemical reactions.

Oxygen content on the surface was reduced by about 8% due to bond breaking and preferential removal of oxygen. The alignment of wall and ripple ridges is
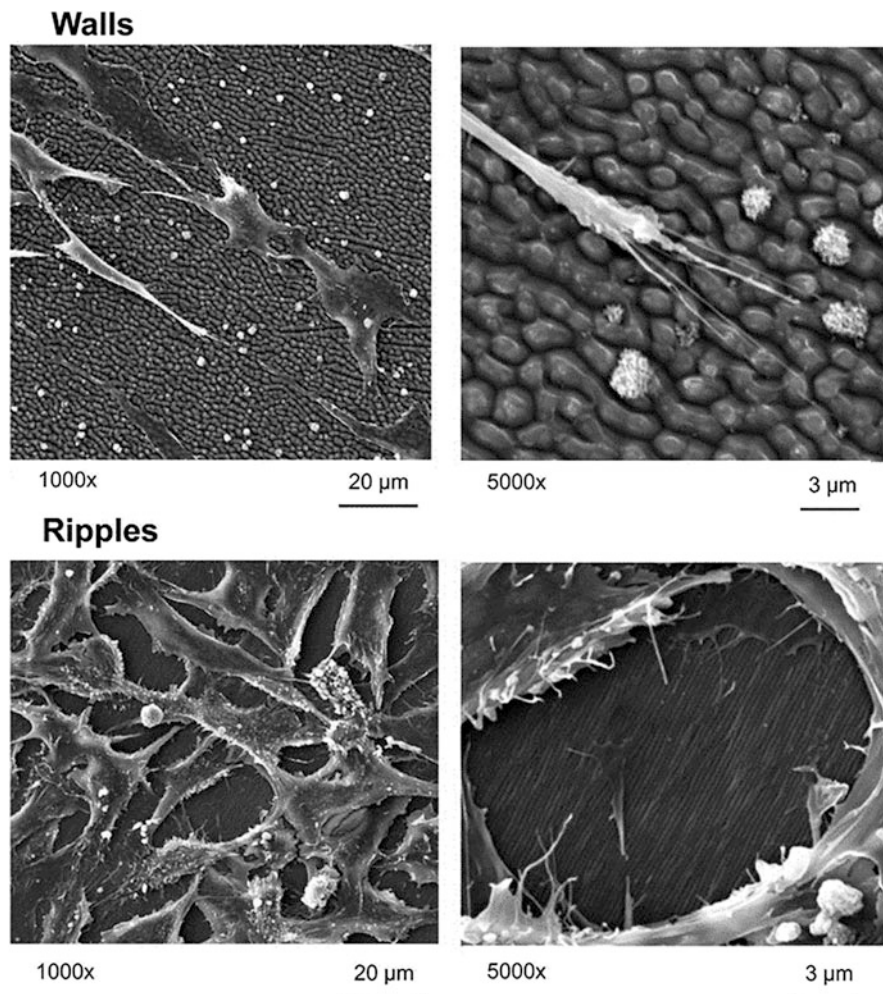
Walls

1000x   20 µm   5000x   3 µm

Ripples

1000x   20 µm   5000x   3 µm

Fig. 31.6 SEM image of HMECs on micro-metric wall-like structures (top) and nano-metric ripple structures (bottom): The cells show alignment on the micro-sized walls, while on the ripples they follow no preferred direction. Even though no alignment is shown for ripples, proliferation of HMECs is nevertheless achieved by relocation of β-catenin to the nucleus instead of the interface regions between the cells. (Reprinted from Schernthaner et al. [101], Copyright (2012), with permission from Elsevier)

perpendicular to the direction of the maximum of the internal stress fields, which originate from the biaxial stretching during the production process of the PET foils. CHO cells align along the direction of the underlying walls and naps and have a spindle-shaped structure.

Guiding cells via micrometer surface texturing has also proven to be an efficient way to increase contact between implanted devices and the surrounding body part.
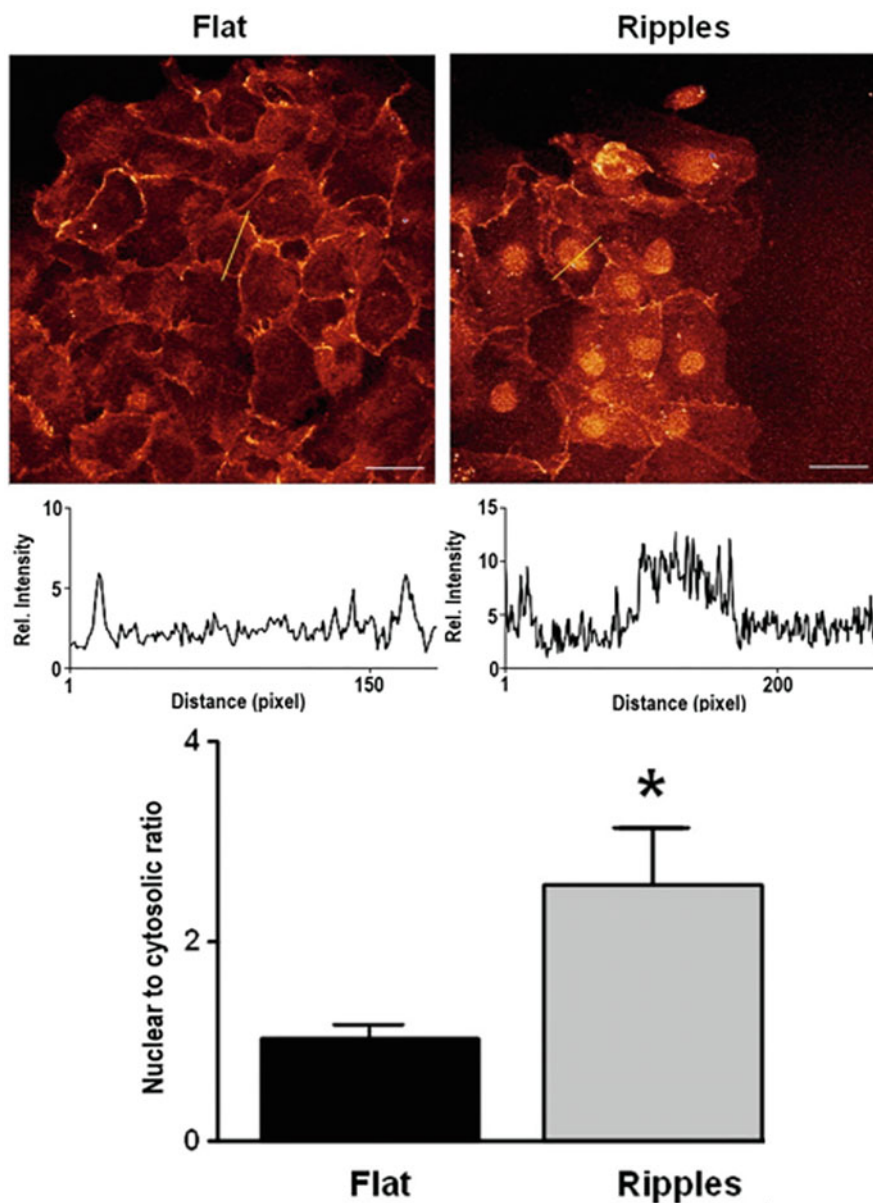
Fig. 31.7 Confocal microscope image of vascular progenitor cells on (left) unstructured and (right) PET foils with ripples: The images and the box plots at the bottom indicate the location of β-catenin in the nucleus for the structured PET substrate. (Reprinted from Schernthaner et al. [101], Copyright (2012), with permission from Elsevier)
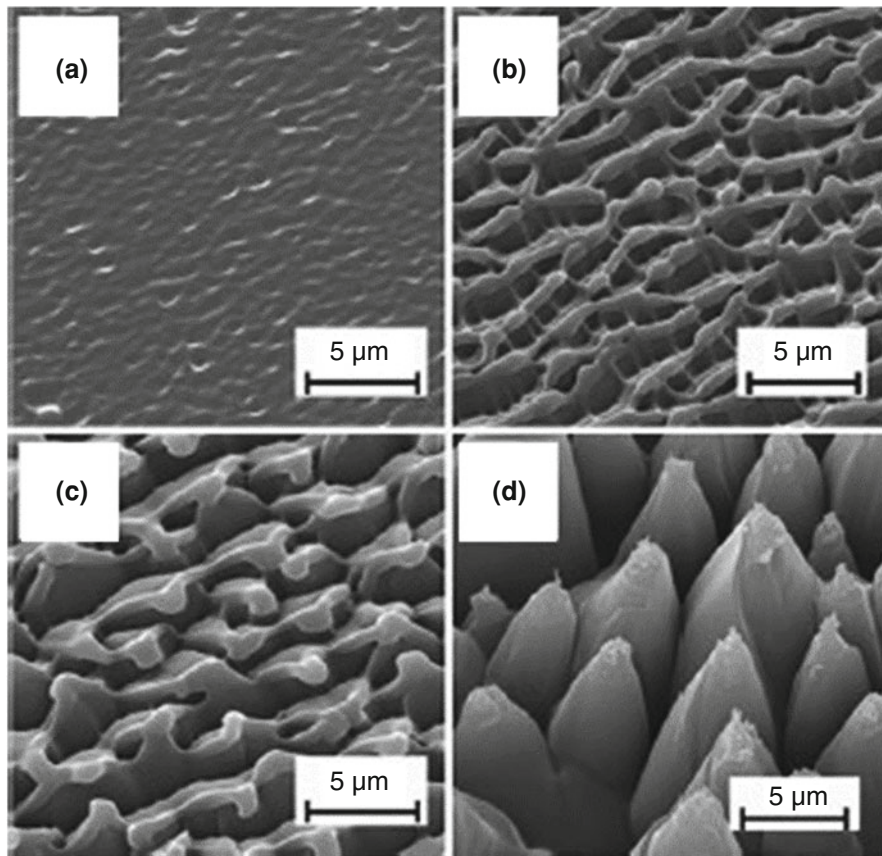
Fig. 31.8 SEM images of (**a**) ripple-like structures (10 pulses), (**b**) wall-like structures (25 pulses), (**c**) nap-like structures (50 pulses), and (**d**) cone-like structures (600 pulses) fabricated by EUV irradiation. (Reprinted by permission from Springer Nature: Reisinger et al. [105], Copyright (2010))

This has been proven to be significant for auditory implants, where a high contact area between the platinum electrodes of the implant and the ear is necessary to provide an excellent hearing experience [108–110]. These implants are constituted from a silicone elastomer which contains several platinum electrode lines that function as inner hair cells, which convert mechanical vibrations into electric signals. Furthermore, auditory implants are also subjected to connective tissue ingrowth, which leads to an increased transitory resistance and interferes with an optimal nerve-electrode interaction [111, 112]. Therefore, Reich et al. [113] investigated the ability of guiding neuronal cells in the direction of the platinum contact material by fabricating linear microgrooves on silicone elastomer and platinum samples by laser irradiation. PC-12 cells (a mixture of neuroblastic and eosinophilic cells) and spinal ganglion cells (SGCs) were seeded on both materials, and the development

of neuronal extensions was investigated. Regarding the neuronal extension growth for silicone, it was shown that the molded micro-structured surface has a strong influence on neurite orientation, leading to a growth parallel to the grooves. Laser-ablated micro-structured silicone, however, showed no significant influence on both cell types. It was concluded that micro-structuring offers a possibility of guiding neurites; hereby, the direction of the microgrooves determines the attachment and guidance of the neuronal extensions.

In this subsection, the authors have discussed cell behavior control on various substrates by laser irradiation. Cell behavior control by surface modification has been extensively researched to be used for medical implants. It can be used for alignment of cells in hearing implants [113] and can further be employed in the field of orthopedic and dental implants for better integration into the body [114]. However, laser structuring of implant surfaces can additionally be exploited to achieve a repelling effect, which is in detail discussed in Sect. 2.2.

2.2 Repellent and Anti-adhesive Structures for Medical Implants and Antimicrobiotic Surfaces

As mentioned in Sect. 2.1, biological matter response to a surface can be altered with laser irradiation. This is not only used to align and activate cell growth but also to achieve reduced attachment and growth of cells and bacteria. This, again, is highly favorable in the field of medical implants. Certain implants need to be explanted from the body after a certain amount of time. Examples of implants that need to be removed are pacemakers [115] and bone implants [116]. The effective usage time of pacemakers is limited by the lifetime of the battery, which is several years. For the bone implants, the usage time is limited to several weeks or months, mainly depending on the healing time of the bone fracture. However, by the time of the explantation, these implants are overgrown by confluent multilayers of cells, which, when activated, produce a layer of ECM that encapsulates the implant. This can make the removal difficult due to the possibility of damaging the body part the devices are implanted into [117]. It is therefore desirable to avoid attachment of cells to be able to remove these devices after their respective lifetimes.

As in the case of cell alignment and activation processes, several combinations of physical and chemical modifications of surfaces have been investigated to achieve the desired cell-repellent properties [25, 116, 118, 119]. Qi et al. [118] investigated the blood-biomaterial interaction and evolution of surface modification for cardiovascular devices. In the past several years, the cell behavior on femtosecond laser-induced hierarchical titanium surface micro-/nanostructures was investigated. Titanium and its alloys are the most prominent materials in implant devices [120] and are extensively employed for pacemakers, bone implants, and dental implants [25, 114, 116, 119, 121]. Titanium, like other valve metals, forms a natural thin oxide layer, which can be thickened by anodization [122, 123].
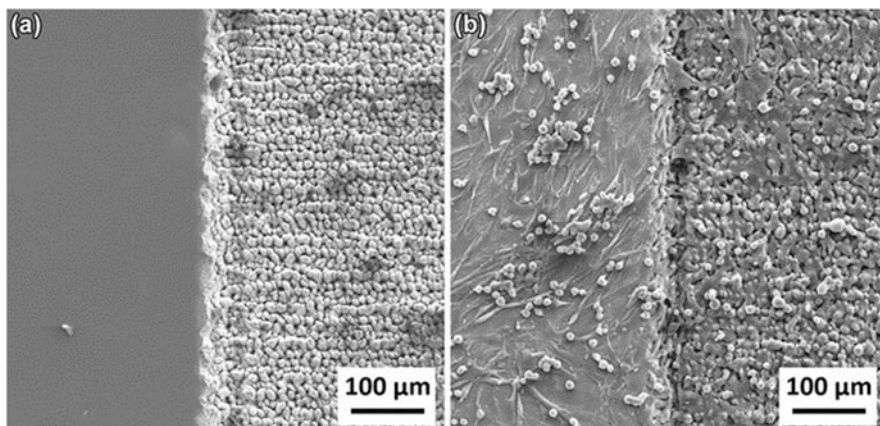
Fig. 31.9 SEM images of the rim between flat, anodized titanium alloy and laser-structured, anodized titanium alloy surface with (**a**) the surface before cell seeding and (**b**) the fibroblasts 1 week after seeding. (Reprinted from Heitz et al. [25], which is licensed under Creative Commons Attribution 4.0 International License (http://creativecommons.org/licenses/by/4.0/))

The interest of using combinations of micro- and nanostructures for cell behavior control on titanium surfaces was sparked by Ranella et al. [72], where femtosecond laser-induced structures were fabricated for cell adhesion tuning on silicon. It is assumed that the combination of both morphological types decreases the effective contact area and limits the number of focal adhesions on the tips of the spikes. Additionally, chemically modifying the surface was found to decrease the adsorption of specific ECM proteins, therefore leading to decreased cell growth (Fig. 31.9). Fibroblast adhesion reduction was successfully achieved on flat titanium samples, which were laser-structured and subsequently electrochemically anodized. In Fig. 31.9, the rim between an unstructured and a laser-structured titanium alloy surface is shown. Both, the unstructured surface and the micro-/nanostructures, were additionally electrochemically anodized. The left image (a) shows the surface before seeding with fibroblasts and the right image (b) the titanium surface 1 week after fibroblast seeding. On the flat, anodized surface the fibroblasts grow in confluent multilayers, while on the laser-structured and anodized surface, only a few adherent cells can be found. It was also reported that the cells change their shape if they do not adhere to the surface below, resulting in spherically shaped cells.

This principle was then used to achieve cell-repellent rings on cylindrical titanium samples. In Fosodeder et al. [119], titanium cylinders with 8 mm diameter were structured by a titanium sapphire (Ti:Sapphire) femtosecond laser system to achieve rings of self-organized structures (Fig. 31.10). These cylinders were subsequently electrochemically anodized by using the sample as a working electrode and dipping it into the electrolyte. This resulted in anodized titanium surfaces surrounding the laser-structured, anodized ring. Fibroblast cell tests were performed by placing the cylinder upright in the Petri dish with the cell culture medium in a
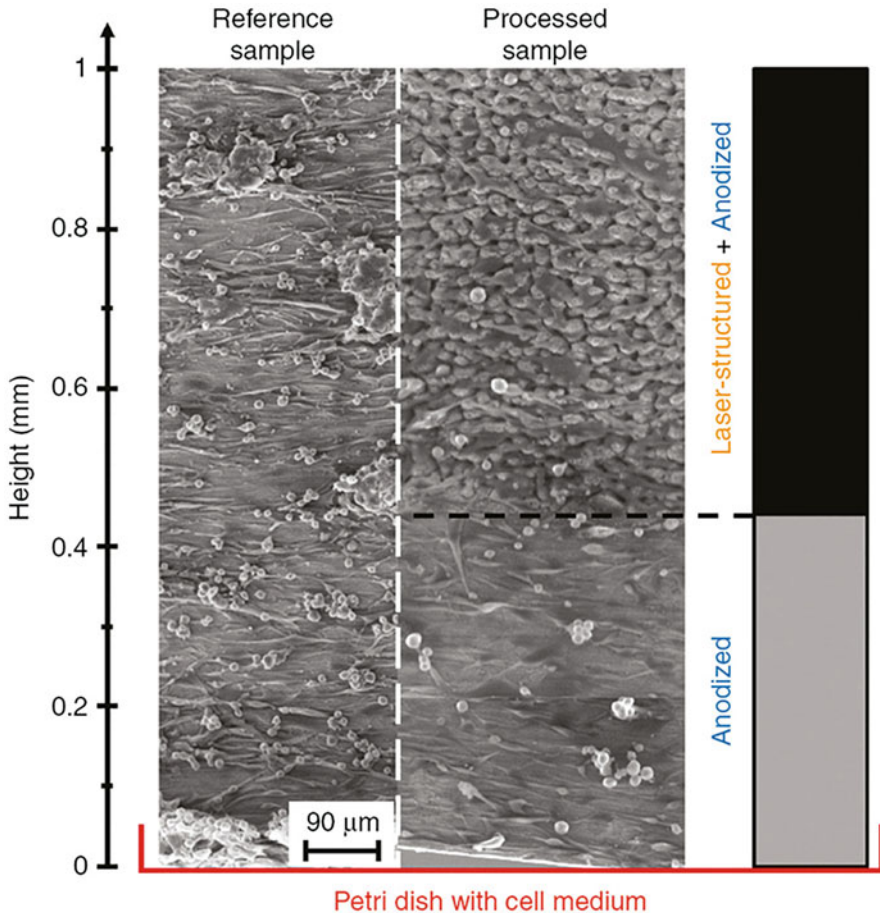
Fig. 31.10 SEM images of a cylindrical control sample (left) and an anodized cylinder with a laser-structured ring at a height of about 400 μm (right). While the control sample shows confluent fibroblast multilayers up to 1 mm height, the laser-structured ring gradually reduces the cell growth until it stops after a few hundreds of micrometers. (Reprinted from Fosodeder et al. [119], which is licensed under Creative Commons Attribution 4.0 Public License)

way that its end closer to the ring is placed in the Petri dish, and an additional control cylinder, which was neither laser-structured nor electrochemically anodized, was also placed in the Petri dish. In Fig. 31.10, it is shown that for the control sample, the cells climb in confluent multilayers up to 1 mm, while on the structured and anodized cylinder, the fibroblast density starts to decrease when they reach the laser-structured ring, up to the point where only a few cells remain after a few hundreds of micrometers. This leads to the assumption that laser-structured and anodized rings can also be used on pacemakers to achieve cell repellency and simplify the removal process.

Lone et al. [63] investigated the electrochemical surface area (ECSA) of structured titanium surfaces. They reported that the ECSA is determined by the voltage used for electrochemical anodization due to electrowetting. At low voltages the electrolyte does not penetrate the structured surface enough to be able to be detected. At higher voltages the electrolyte penetrates the surface structures, leading to an increased ECSA and oxygen evolution. It was also shown that the relative weight percentages of titanium, aluminum, and vanadium in the titanium alloy Ti6Al4V-ELI (extra low interstitial) change after laser treatment and/or anodization due to effects resulting from different evaporation temperatures and passivation.

It is further known that mesenchymal stem cells (MSCs) present in the bone marrow respond to metal implants by forming soft tissue rather than bone, which results in failure of load-bearing prosthesis. Structuring of implant materials such as titanium can be used to differentiate stem cells into the desired cell type. Böker et al. [124] investigated various nano-topographies on PS, stainless steel, and titanium samples. It was observed that a significant reduction of osteocalcin (OCN) expression on structured stainless steel and titanium surfaces occurred compared to non-structured surfaces. It was concluded that the gene expression depends on the underlying structure type. It is also possible to nanopattern surfaces by electron beam lithography (EBL). Dalby et al. [125] produced different nanoscale patterns, concluding that the design and the size of the nanopattern determine the differentiation of MSCs into cells with fibroblastic and osteoblastic morphology.

Due to increased usage of medical implants, implant-associated infections also increased, leading to expensive health-care costs and follow-up treatments for the patient [126, 127]. Implant-associated infections are caused by bacterial biofilms, which form via attachment of bacterial cells and subsequent formation of a polysaccharide matrix, which functions as a protection medium for bacteria. Once biofilms develop, they show exceptional resistance mechanisms against antibiotics and antibacterial coatings applied before implantation [128].

It is therefore desirable to hinder the formation of biofilms by preventing ab initio attachment of bacteria. Several species, such as cicadas and dragonflies, developed nano-sized structures on their wings to hinder the attachment of bacteria [129–131]. Bacterial adhesion is influenced by factors such as species, implant material, environmental aspects, and physical and chemical properties of the implant surfaces [132]. In the process of attachment, bacteria adhere to the surface by increasing the contact area to the underlying substrate as far as possible, extensively stretching the bacteria membrane. Same as cells, bacteria are therefore highly influenced by surface topographies, eventually leading to rupturing of the bacteria membrane if the stretching threshold is exceeded.

An example for bacteria rupturing on two different types of surfaces with ripples is shown in Fig. 31.11 [133]. Furthermore, bacterial attachment is also governed by surface chemistry and wettability, so a combined approach of physical and chemical modification of medical implant surfaces can lead to an antibacterial effect. Nano-sized structures will eventually penetrate the bacteria wall, causing them to rupture, and micro-sized structures will strongly reduce the available flat contact area, preventing the attachment of bacteria.
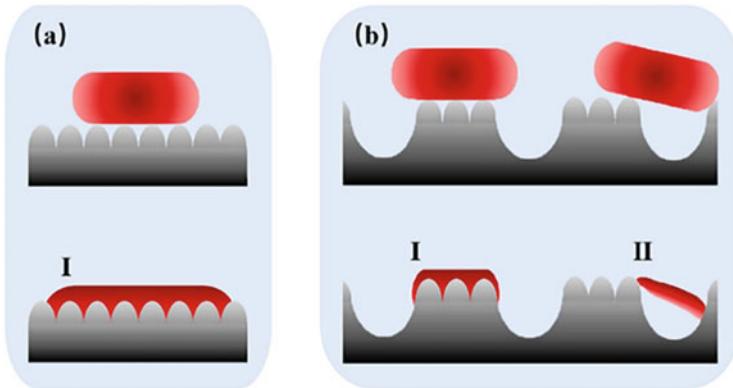
Fig. 31.11 Bacterial cell rupturing mechanism demonstrated on (**a**) a platy form and (**b**) a lacerated form. (Reprinted from Luo et al. [133], Copyright (2020), with permission from Elsevier)

It has been shown that stand-alone chemical modification, for example, by applying antibacterial coatings, fails with respect to long-term performance [134], and therefore a combined approach of both physical and chemical modification is required [135]. Morphologies on the nanometer scale such as nanowires, nanopillars, and nanotubes were investigated and found to increase the antibacterial properties of implants [136–138]. However, it was further proposed that additional treatment of the nano-sized structures, such as heat treatment or polymer coating [139–141], has to be applied to achieve the desired biocompatibility. Laser-induced periodic surface structures (LIPSS) were therefore investigated due to the possibility of producing antibacterial surfaces in a cost-effective and fast way while avoiding surface contamination. Similar as for cells, LIPSS limit the available area for bacterial attachment and are therefore highly promising structures to create antibacterial medical implant surfaces.

Epperlein et al. [142] investigated the adhesion of *Staphylococcus aureus* (*S. aureus*) and *Escherichia coli* (*E. coli*) on LIPSS generated on steel substrates. They found out that *E. coli* adhesion is highly affected by laser-induced structures, while the adhesion of *S. aureus* is not affected by LIPSS. Schwibbert et al. [143] investigated bacterial colonization of *S. aureus* and *E. coli* on femtosecond laser-induced sub-μm structures generated on poly(ethylene) (PE) substrates. However, here the generated structures were no LIPSS. It was shown that *S. aureus* adhesion was not reduced on the fabricated structures, but that the presence of laser-induced structures had a significant effect on the adhesion of *E. coli*. In Richter et al. [70], it was demonstrated that the spatial period of LIPSS on PET polymer foils determines *E. coli* repellence. SEM and biofilm studies using a pili-deficient *E. coli* TG1 strain revealed the role of extracellular appendages in the bacterial repellence.

Slippery, liquid-infused porous surfaces (SLIPS) generated by laser irradiation, chemical modification, and subsequent infusion with lubricants investigated by Doll et al. [144] were introduced as another method to inhibit bacterial attachment (Fig.
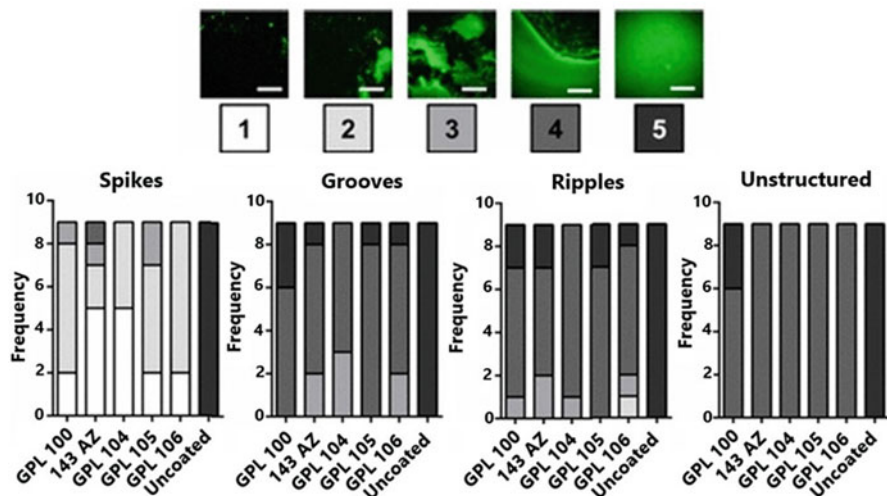
Fig. 31.12 *S. oralis* biofilm formation screening on titanium SLIPS with varying structure/lubricant combinations: The level of biofilm formation is categorized into five groups: level (1) means nearly no bacterial film and level (5) means complete coverage of structures with biofilm. The corresponding levels of coverage for each structure type are demonstrated in the box plots. (Reprinted (adapted) with permission from Doll et al. [144]. Copyright 2017 American Chemical Society)

31.12). Three main criteria have to be fulfilled to achieve the desired outcome: (1) the lubricant has to adhere stably to the surface, (2) the surface must be preferentially wetted by the lubricant rather than by the repellent liquid, and (3) the lubricant and the repellent liquid must be immiscible [145]. Spikes, grooves, and ripples were fabricated on titanium by fs-laser structuring and subsequently dip-coated by a fluorinated polymer as chemical modification. The structures were then spin-coated with five different perfluoropolyether lubricants with varying viscosities. For testing of biofilm-repellent properties, the structures were subjected to *Streptococcus oralis* (*S. oralis*). The level of surface coverage was divided into five groups (1–5), where (1) means nearly no biofilm formation and (5) means complete surface coverage by the biofilm. While spike SLIPS showed nearly no or very small biofilm fragments (level (1)), ripples, grooves, and unstructured surfaces exhibited partially or complete coverage by *S. oralis* biofilms (level (4) or (5)). However, all structured surfaces showed a reduction of biofilm formation compared to the unstructured surface. Additionally, all uncoated structures showed level (5) biofilm formation, meaning that only the combination of structures and lubricants serves as an efficient biofilm-repellent tool. As it can be seen in Fig. 31.12, the biofilm surface coverage for unstructured titanium is almost the same for all lubricants, while all structured surfaces showed at least partial bacteria reduction, with spike structures providing the best results.

It is also worth mentioning that cell-repellent properties have not only been achieved with self-organized structures but also with the process of TPP. Paun et al. [146] created mushroom-like structures that feature ripples in the μm and nm range. They concluded that the nano-metric ripples on top of the mushrooms had much more influence on the cellular attachment than the micrometer-sized structures. They also investigated the influence of wettability on the cell adhesion and found that cell attachment was mostly affected by the surface topography. The cells used in this work were from an oligodendroglia cell line (OLN-93 cells) that has been derived from primary rat brain glial cultures.

2.3   Cell Arrays and Scaffolds for Tissue Engineering Applications

Two-photon lithography (see Sect. 1.2), is a powerful and versatile tool [32, 147, 148], which found multiple applications in the study of cells, as it offers the opportunity to build microenvironments onto which cells can be seeded and their behavior can be analyzed. In this subsection, the authors aim to present an overview on the vast field of possible applications of TPP in the study of cells. Tissue engineering (TE) [149–151], as a biomedical engineering field, uses cells, scaffolds, and appropriate bioactive molecules to produce functional tissue in order to restore, maintain, improve, or replace damaged tissue. Cell scaffolds are responsible to mimic the native ECM of tissue [152]. The ECM is a 3D network of proteins and carbohydrates which provides structural and biochemical support to surrounding cells [153]. Each tissue has a specific ECM composition and topology, but it always regulates cell differentiation, proliferation, migration, and adhesion. In order to artificially produce a functional tissue, the cell supporting structures need to be as close as possible to the natural ECM. Due to its inherent true 3D printing capabilities, TPP is widely used in the production of artificial cell scaffolds [152]. Some of the most common geometries implemented for cell scaffolds are woodpiles [154–156], squares [157–159], honeycombs [160–162], and circular/tubular geometries [163–165]. In these cases, TPP technique offers the possibility to produce scaffolds of arbitrary shapes with control over the pore sizes and feature sizes both in the lateral and axial directions.

Numerous cell types have been studied using TPP scaffolds: osteoblasts [161, 163, 166], fibroblasts [167, 168], chondrocytes [169, 170], endothelial cells [162, 171], neuronal cells [155, 164], stem cells [38, 172], retinal cells [165, 173], etc. For TE applications, the materials used for building the scaffolds have to be biocompatible (the material has to be nontoxic and harmless for the cells) and sometimes biodegradable (the material needs to be decomposable with nontoxic by-products). Commercially available synthetic biocompatible materials that are used for cell studies are Ormocer® such as OrmoComp® and SU-8 [174], acrylate-based SCR500 and epoxy-based SZ2080 (20/80 zirconium-silicon/methacrylate sol-gel,

containing 4,4'-bis (diethylaminobenzophenone)), and Norland Optical Adhesive 61 (NOA 61) [37]. Natural materials that can be used for TPL scaffolds are sodium hyaluronate (SH), chitosan [175], hyaluronic acid [37], etc. The synthetic photoresists have outstanding and tunable mechanical properties; therefore, a combination of synthetic and natural photoresists is advantageous.

To study the influence of pore sizes on cell proliferation, OrmoComp® TPP scaffolds with pore sizes varying from 10 to 90 µm were produced, and human dermal fibroblasts were seeded on them [167]. By observing the cell behavior 3, 6, and 9 days after seeding, it has been reported that the scaffolds with larger pores (90 µm) aided to a higher cell growth and proliferation. Also, the scaffolds with 10 µm pores promoted cell alignment along the prominent lines of the scaffold, which was not observed for scaffolds with bigger pore sizes. Comparing the effect of different pore sizes (12 µm, 25 µm, 52 µm, and 110 µm) on cell migration, another study reported that human fibrosarcoma cells of the HT1080 cell line cells move with higher speeds on triacrylate 3D scaffolds compared to the 2D substrate [154]. For smaller pore sizes, a slower speed was observed due to more obstacles the 3D matrix imposed.

The two new biocompatible polymers M10 and BisSR, which can be 3D structured via multiphoton lithography, were tested mechanically by AFM, and their biocompatibilities were compared to pentaerythritol tetraacrylate (PETA) and OrmoComp® [176]. Assessment of biocompatibility of the new resins was done by cultivating human umbilical vein endothelial cells (HUVECs) on 2D grid structures for 4 days; then cell density and presence of apoptotic cells were measured. This analysis indicated a better biocompatibility of the two new photoresists BisSR and M10 compared to PETA and OrmoComp®.

Honeycomb geometries produced with TPP, arranged in a multilayer configuration, are used to aid the 3D attachment and growth of MG-63 osteoblast-like cells, as they mimic the natural bone structure [161]. The authors compared how different distances between consecutive layers affected cells and concluded that for a spacing of 2–10 µm, the cells are able to penetrate between individual layers, interconnect with each other, and promote formation of mineralized tissue. For layer spacings lower than 2 µm and higher than 10 µm, this behavior was not observed. This geometrical configuration is believed to facilitate cell interconnections, to support cellular metabolism through vascularization and nutrient transport to the cells, and to allow easy nerve access to the cells.

In [177], polymer microstructures with one or more levels of quadratic pores were written onto a flexible substrate by TPP (Fig. 31.13). Primary human nonbulbar dermal sheath (NBDS) fibroblast cells served as progenitor cells. They differentiated into an osteogenic lineage and were seeded onto the hydrophilic three-dimensional scaffolds. Due to confinement to the microstructures and/or mechanical interaction with the scaffold, the cells were stimulated to produce high amounts of calcium-binding proteins, such as collagen type I, and show an increased activation of the actin cytoskeleton. The best results were obtained for quadratic pore sizes of 35 µm. Further examples for cell scaffolds produced by laser-assisted techniques for tissue engineering applications are described in the Refs. [178, 179].
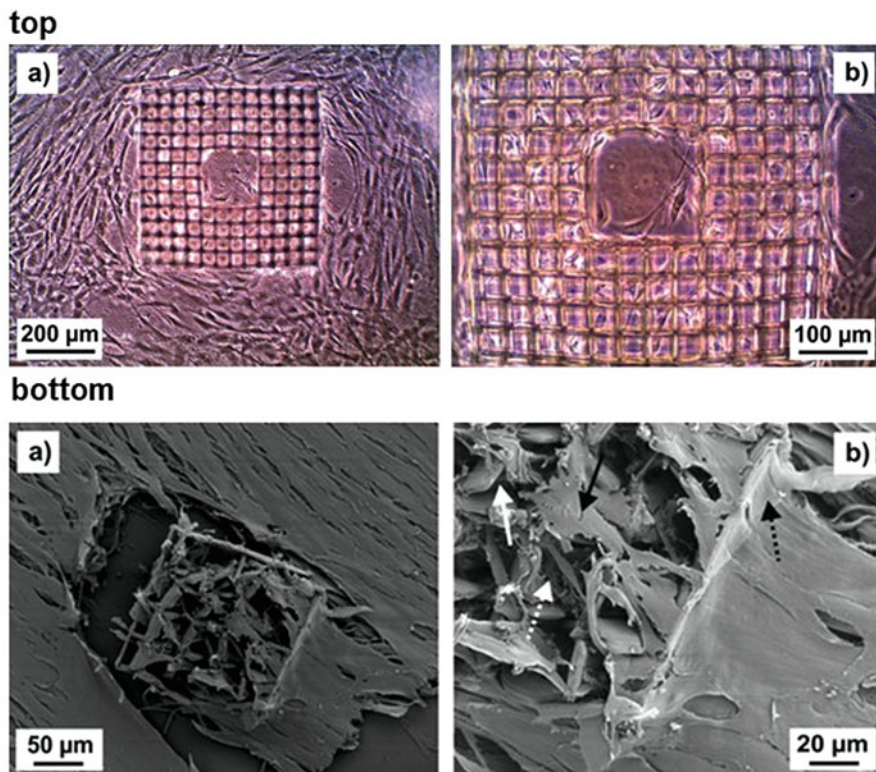
Fig. 31.13 Optical microscope images (top (**a**) and (**b**)) and SEM images (bottom (**a**) and (**b**)) of low (**a**) and high (**b**) magnifications of a cage microstructure with 35 μm square pores on a flexible polymer substrate seeded with NBDS fibroblast cells and cultured in osteogenic culture medium. In (**b**) at the bottom, the solid white arrow points to part of a pore sidewall, the solid black arrow to a cell inside the structure, the dashed white arrow to an area which is rich in fibrous extracellular material, and the dashed black arrow to a cell part at the outer rim of the structure. (Reprinted from Heitz et al. [177] with permission from Wiley. ©2016 The Authors. Journal of Biomedical Materials Research Part A Published by Wiley Periodicals, Inc.)

Three-dimensional blood vessel analogues with a honeycomb cell unit were as well tested for adhesion and proliferation of HUVECs (Fig. 31.14) [162]. The geometrical parameters of the scaffolds were obtained by simulating the mechanical response to external stresses applied to the scaffolds' sidewall structure with a finite element analysis (FEA), and TPP was implemented to create a cylindrical hollow scaffold (100 μm wide and 80 μm tall) with honeycomb wall pattern. A single hexagonal unit cell had a thickness of 5 μm, a side length of 3 μm, and a cell wall width of 1 μm. Upon cell seeding, the artificial vessel proved to sustain large elastic forces. It is expected that in further in vivo studies, the scaffolds would have a proper elastic behavior to withstand the pressure exerted by blood flow.
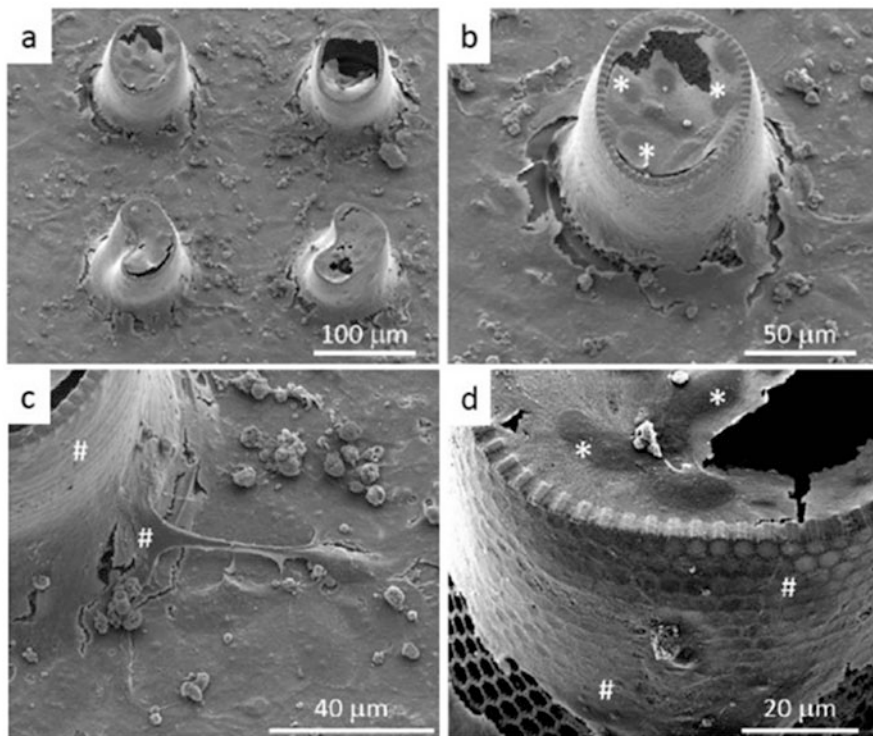
Fig. 31.14 Representative low-magnification (**a**, **b**) and high-magnification (**c**, **d**) SEM images of HUVECs grown in vitro for 9 days on tissue-engineered vascular grafts. (Reprinted from Limongi et al. [162], which is licensed under Creative Commons Attribution 4.0 license; http://creativecommons.org/licenses/by/4.0/)

By repeating the lithographic process with different photoresists, complex micro-sized structures with distinct chemical properties were produced [180]. An array of pillars ($\approx 7\ \mu m$ in diameter, $\approx 23\ \mu m$ in height) connected by beams ($1\ \mu m$ in diameter) was created using TPP from poly(ethylene glycol diacrylate) (PEG-DA) and PETA mixture. After development of the array, the pillars were cast with a second photoresist (OrmoComp®) and cubes ($2.5\ \mu m$ edge length) were written onto the middle beams connecting two adjacent pillars. After a second developing step, the arrays were incubated in FN solution, which promotes cell adhesion. Upon seeding the arrays with chicken fibroblasts, it was observed that cells bind specifically to the OrmoComp® cubes, as PEG-DA is protein-repellent. The authors proved that by using protein-binding sites embedded on a protein-repellent array, cell adhesion and consequently cell shape can be controlled in a 3D manner.

Besides FN, other chemical treatments and coatings can be used to enhance cell adhesion. As an example, TPP was employed to produce arrays combining hollow posts and rods in order to study the influence of chemically homogeneous

3D topographies on osteoblast-like cell proliferation [181]. The posts were 12 µm high and 10 µm wide, while the rods were about 1.5 µm high and 0.45 µm wide. Commercially available acrylate-based IP-L 780 was used as a photoresist. After the developing step, to assure biocompatibility and homogeneity of the array and its substrate, each sample was coated with a thin layer of titanium oxide using atomic layer deposition (ALD), and osteoblast-like cells were seeded onto the arrays. A 170% increase in proliferation of osteoblasts was observed compared to unstructured titanium dioxide surfaces, when the posts were placed 25 µm apart. The cells also showed a higher content of alkaline phosphatase, which is an enzyme related to bone mineralization.

In conclusion, TPP allows overcoming the major disadvantages of other 3D structuring techniques by enabling the creation of intricate real 3D microenvironments that mimic the ECM. For further information, the reader is encouraged to check the following reviews [147, 148, 152].

2.4 Microneedles for Drug/Vaccine Delivery

Microneedles (MNs) are systems of micron-sized needles [182] organized in arrays covering surfaces up to square centimeters [183]. Due to their short lengths, MNs penetrate only into the top layers of the skin [184], that is, the stratum corneum and the epidermis, without irritating the nerve endings or reaching the blood vessels that lie deeper in the dermis [185]. Hence, MNs are minimally invasive tools, which do neither trigger pain sensations nor induce bleeding [186], used for wide-ranging applications such as transdermal drug and vaccine delivery, drug monitoring [187], sample extraction for diagnosis [188], and real-time monitoring [189, 190]. Depending on the mechanism of drug delivery, MNs are classified in five categories: solid, hollow, coated, dissolving and hydrogel-forming, or swellable [191]. In this subsection the authors focus on the use of TPP in the production of MNs [192, 193]. The authors aim to present a summary of the large amount of MNs and MN arrays that can be fabricated using the TPP technique. TPP is mainly used to produce solid [194], hollow [159, 195], and coated MNs [196] (Fig. 31.15). Furthermore, the solid arrays can be used as master templates for negative molds. The latter ones can be used to mass-produce dissolving [197] and hydrogel-forming MN arrays [192]. Regardless of their more complex geometry, even hollow MNs can be reproduced with high fidelity using micro-molding techniques [196, 198].

MNs with smaller tip diameter were found to penetrate the skin more smoothly than MNs with a larger tip diameter [184]. A decrease in the MN aspect ratio (height to base diameter) also results in an increased mechanical strength [194]. Besides, MN arrays are more resistant to fracturing during penetration than single MN, as the shear stress created by the tissue is distributed over a larger area [199]. These considerations are relevant when designing and producing a MN, since MN patches are desired to be applied with minimal effort and no damage to the skin or to MNs themselves. Furthermore, these requirements translate into parameters
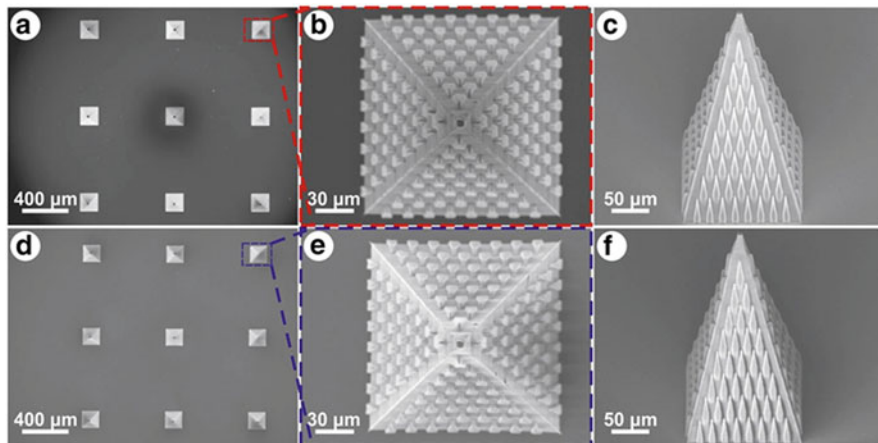
Fig. 31.15 SEM micrographs of a 3 × 3 MN array of (**a**) the TPP original and (**d**) its corresponding epoxy replica. SEM micrograph of a TPP-structured MN from the 3 × 3 array: (**b**) top view and (**c**) side view. SEM micrograph of an epoxy-replicated structured MN: (**e**) top view and (**f**) side view. (Reprinted from Plamadeala et al. [196], which is licensed under Creative Commons Attribution 4.0 International License; http://creativecommons.org/licenses/by/4.0/)

easily controllable through the use of TPP in MN production. This technique offers flexibility in adjusting MN aspect ratios, tip opening angles, and tip diameters [159, 200, 201] as well as adjusting the MN density within the array area.

The excellence of TPP in the production of real 3D structures is evident especially in the achievable designs of hollow MNs [174, 195, 198]. Arrays of in-plane and out-of-plane MNs with different aspect ratios were produced and tested for their fracture and penetration properties [174]. Square arrays of 25 MNs with 500 µm spacing were produced using the Ormocer® photoresist. Three types of MNs with different pore positions were designed: 0 µm (the opening is situated right on the tip of the MN), 1.4 µm, and 20.4 µm off-center, respectively. During penetration tests, the latter MN design proved to exert the lowest resistance upon penetration due to having the sharpest tip. A higher mechanical strength was also observed in MNs with larger base diameter. This study offers practical insights into a proper MN design for an increased mechanical stability during penetration.

Coating MNs with the desired drug formulation implies the use of another setup in an extra production step, which is often time- and finance-consuming [191]. By using TPP, the coating step can be simplified by incorporating microfluidic channels on the MNs and/or in the MN array [196]. Using TPP to create structured guiding channels between MNs and on the MNs' lateral sides, it has been shown that the latter is easily coated with a liquid formulation compared to a MN with smooth lateral sides. In the case of hollow MNs, TPP proved to be essential in conveniently designing and producing MNs with one open microfluidic channel

along its body side [198]. By connecting the open channels of each individual MN into a reservoir, the array can be used for collecting and analyzing body liquids in diagnostic applications. These geometrical features of functional relevance are beyond what is achievable with any other fabrication method.

Concluding this subsection, TPP has allowed creating MNs of user-defined designs with sub-micron features of various complex geometries. For further information, the reader is encouraged to check the following reviews [182, 193].
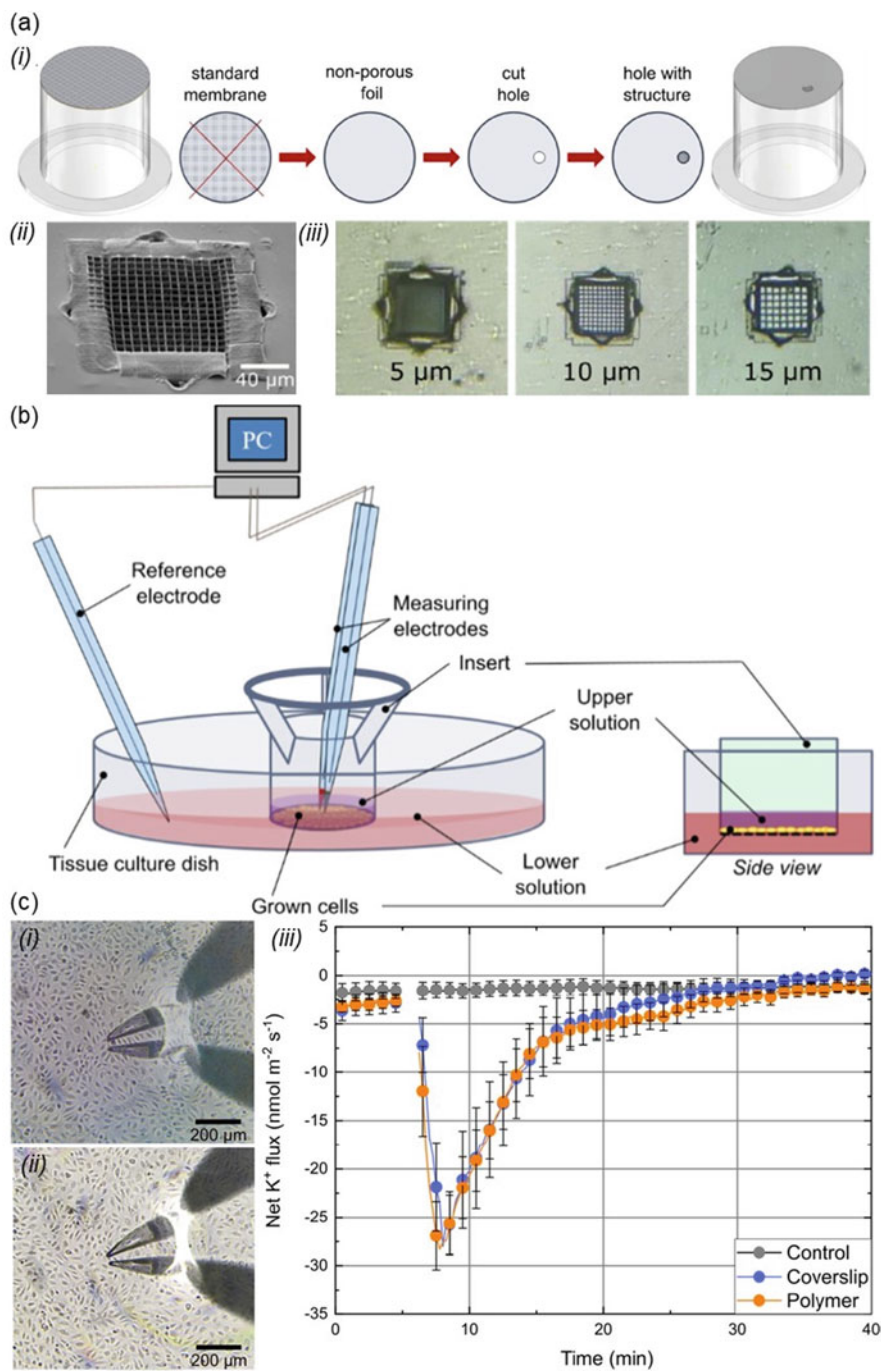
2.5 Micro- and Nanostructures for Fluidic Systems and Analysis Techniques

Three-dimensional photopolymerization techniques such as multiphoton lithography (MPL) and specifically TPP [32, 196, 202–205] and STED [206, 207] are tools for fabricating structures in the sub-μm range (see also "1.2 Direct Writing" for a brief overview on MPL, TPP, and STED). Combining these techniques with microfluidics allows to broaden the range of their applications [196, 202, 203, 207].

Buchroithner et al. [203] developed an improved transwell design for micro-electrode ion flux estimation (MIFE), which is a noninvasive electrophysiological method for cellular membrane transport studies (Fig. 31.16a, b). To this end, they modified a standard transwell membrane by subtractive and additive fs-laser manufacturing (Fig. 31.16a): a measurement window was cut out with a fs-laser beam, into which a 3D grid structure was produced by TPP, for cell support. On top of the polymer grid, HMECs efficiently grew and maintained their physiological response to calcium, which was measured by MIFE (Fig. 31.16b, c).

Buchegger et al. [207] manufactured a microfluidic device enhanced with TPP structures carrying STED lithography-written nanoanchors that promoted binding of the von Willebrand factor (vWF) (Fig. 31.17). This allowed the study of the impact of vWF on the activation of thrombocytes, which seemed to decrease with the density of the vWF. To this end, fluorescently labeled antibodies were bound to the activated thrombocytes.

Fluorescent observation of cells generally suffers from the limited axial resolution due to the elongated point spread function (PSF) of the microscope optics [204]. A way to eliminate anisotropic resolution is to fuse images recorded from multiple viewing directions achieved mostly by mechanical rotation of the entire sample. In the approach of Vizsnyiczai et al. [204] (Fig. 31.18), multi-view imaging of single cells was implemented by rotating them around an axis perpendicular to the optical axis by means of holographic optical tweezers, wherefore special microtools were fabricated by TPP. The three spheres of these microtools provide trapping sites for three holographic optical traps, while a concave-shaped attachment disk possesses a binding site for spherical cells. By the proposed technique, significant resolution improvement was measured on mitochondria-stained single cells. Similarly, surface-modified complex SU-8 microstructures were used for indirect optical manipulation

(a)

(i) standard membrane → non-porous foil → cut hole → hole with structure

(ii) 40 µm

(iii) 5 µm   10 µm   15 µm

(b)

PC

Reference electrode

Measuring electrodes

Insert

Upper solution

Tissue culture dish

Grown cells

Lower solution

Side view

(c)

(i) 200 µm

(ii) 200 µm

(iii)

Net K⁺ flux (nmol m⁻² s⁻¹) vs Time (min)

Control
Coverslip
Polymer

of single cells with six degrees of freedom [205]. For interested readers, Chap. 30 provides further overview on how miniaturized fluidic devices with nanofeatures can be employed for sensing and diagnostics.

However, not all biomedical applications aim for a reduction in structure size using TPP or STED lithography. In some cases, there is a need for large structured areas of several square centimeters with the capability of (with)holding microliters of water or for targeted, that is, (uni)directional, liquid transport (Figs. 31.19, 31.20, 31.21, 31.22, and 31.23). To this end, inspiration from nature [11, 196, 202, 208–212] was beneficial, namely, mimicking the liquid transport capability of spermathecae of fleas [212] (Fig. 31.19), of the integument of lizards [11, 211, 213, 214] (Fig. 31.20), and of bugs' cuticle [196, 202, 208, 215] (Fig. 31.21, 31.22, and 31.23). To get an overview on bio-inspired laser-structured surfaces in general, the reader is encouraged to read Chap. 25.

Buchberger et al. [211–213] applied a commercial laser engraver with a CO_2 laser source to render surfaces of some square centimeters able to transport microliters of liquid unidirectionally in asymmetric capillary channels (Figs. 31.19 and 31.20). To a certain extent, these devices were capable of unidirectional water transport even against gravity (Fig. 31.20).

Kirner et al. [215] mimicked bug-like surface structures and their fluid transport using ultrashort laser pulse irradiation of steel (Figs. 31.21 and 31.22). To this end, they applied pulses with durations in the fs to ps range of different wavelengths and systematically varied the laser processing parameters (peak fluence, effective number of pulses per spot diameter, surrounding atmosphere, and angle of incidence); a variety of LIPSS structures with different surface morphologies originated, namely, ripples, grooves, and spikes.

Unidirectional liquid transport was achieved by a gradient structure with different surface morphologies. As a possible biomedical application of directional liquid transport, Plamadeala et al. [196, 202] replicated asymmetric features found on cuticle of flat bugs by TPP and applied them to microneedles (see also Sect. 2.4) for efficient drug/vaccine coating (Fig. 31.23).

Fig. 31.16 (**a**) Transwell design for MIFE measurements: (i) The standard membrane is cut from a transwell insert; a nonporous, non-permeable foil is attached, in which a hole is cut by a fs-laser; a grid is structured inside the hole with TPP. (ii) SEM image of the polymer grid structures inside the hole. (iii) Bright-field microscopy images of grids with grid constants of 5–15 μm. (**b**) Scheme of MIFE setup: modified inserts with grown cells are placed into a culture dish. The ion-selective microelectrode is moved between two positions. From the potential differences, concentration differences and the flux of the specific ion are calculated. (**c**) Two ion-selective electrodes situated above HUVECs grown on a (i) coverslip and (ii) on a polymer grid fixed on a coverslip. (iii) Response of HUVECs to calcium ionophore. Solvent (ethanol, gray dots) or calcium ionophore (to 10 μM, orange and blue dots) was added after 5 min to either cells grown on a coverslip (blue dots) or polymer structures (orange dots). (Adapted from Buchroithner et al. [203], which is licensed under the Creative Commons Attribution (CC BY) license (https://creativecommons.org/licenses/by/4.0/))
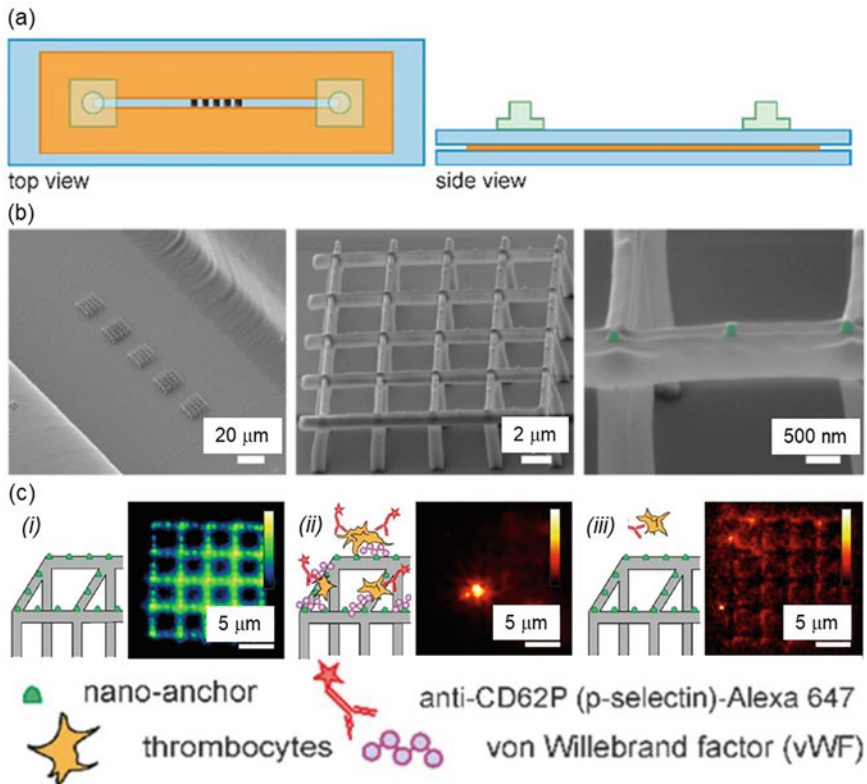
Fig. 31.17 Microfluidic device for thrombocyte activation studies: (**a**) Sketch with top and side view. Blue, glass slides; orange, double-sided adhesive tape; green, in and outlet connectors. (**b**) SEM images of the structures inside the microfluidic channel. Protein-repellent TPP grids on posts (gray) carrying STED lithography-written nanoanchors (green). (**c**) (i) Left: Sketch of the protein-repellent structure (gray) with protein-binding nanoanchors (green). Right: Fluorescence microscopy image of an empty scaffold. (ii) Left: Sketch of the experiment for thrombocyte activation. The protein-binding nanoanchors were labeled with vWf molecules. Subsequently, thrombocytes were added to the microfluidic device. Fluorescently labeled antibodies were bound to the activated thrombocytes. Right: Fluorescence image of activated thrombocytes bound on top of the scaffolds. (iii) Left: Sketch of the control experiment, where vWF molecules were omitted. The structures were incubated with a thrombocyte concentrate under flow conditions and subsequently incubated with fluorescently labeled antibodies. Right: There were no activated thrombocytes present on the structures. (Adapted from Buchegger et al. [207], which is licensed under Creative Commons Attribution 4.0 International License; http://creativecommons.org/licenses/by/4.0/)
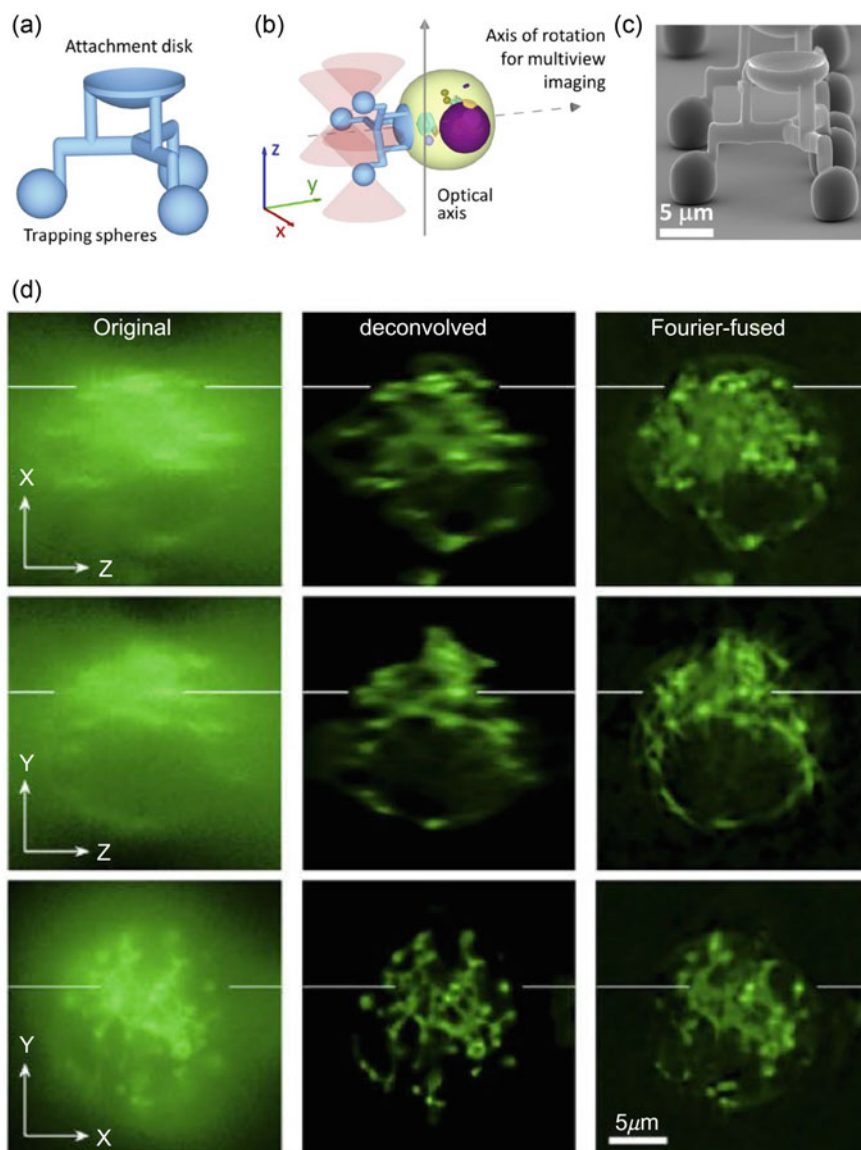
Fig. 31.18 Scheme of a polymer micromanipulator made by TPP and its application to indirectly manipulate a single cell for multi-view microscopy: (**a**) The model of the manipulator showing its main functional parts. Three spheres provide trapping sites for three holographic optical traps, while a concave-shaped attachment disk possesses a binding site for spherical cells. (**b**) The spatial arrangement of the manipulator-cell couple in the sample space relative to the optical axis of the trapping and observing objective. Pink cones indicate the trapping beams. The cell is rotated around the dashed-line axis for the multi-view microscopic observations (parallel to axis *y*). (**c**) SEM image of the cell manipulator structure. (**d**) Resolution improvement measured on mitochondria-stained single cells: Corresponding single slices taken from the original, deconvolved, and fused 3D data arrays (columns) along the three axes (rows). (Adapted with permission from Vizsnyiczai et al. [204] © The Optical Society)
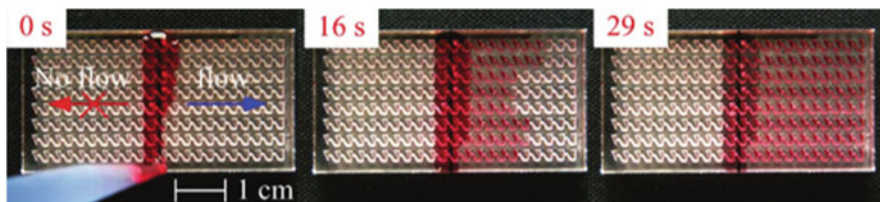
Fig. 31.19 Large-area unidirectional liquid transport bio-inspired by fleas; the capillary channels in poly(methylmethacrylate) (PMMA) were fabricated by means of an industrial CO_2 laser engraver. They are capable of transporting some microliters of liquid. (Reprinted from Buchberger et al. [212], which is licensed under Creative Commons Attribution 4.0 International License (http://creativecommons.org/licenses/by/4.0/))
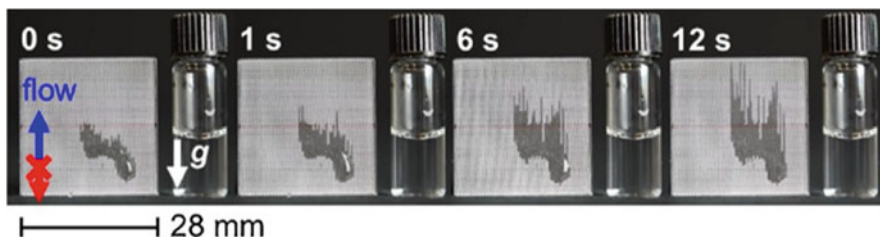

Fig. 31.20 Large-area unidirectional liquid transport mimicking the integument of lizards; the capillary channels in poly(methylmethacrylate) (PMMA) were fabricated by means of an industrial CO_2 laser engraver. They maintain the capability of unidirectional liquid transport even against gravity. (Reprinted from Buchberger et al. [211], Copyright (2019), with permission from Elsevier)
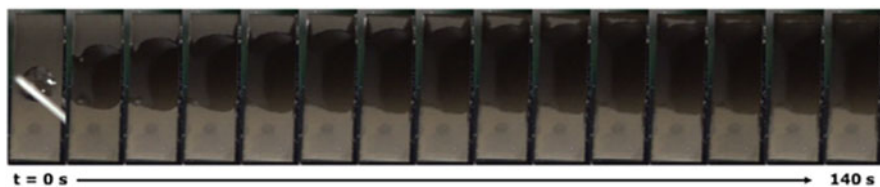

Fig. 31.21 Large-area unidirectional liquid transport bio-inspired by bugs; the image series shows a gradient structure, which possesses different surface morphologies in response to changes in fluence originated from fs-laser processing (area of 8×15 mm^2). (Reprinted by permission from Springer Nature: Kirner et al. [215], Copyright (2017))

2.6 Sensors Based on Micro- and Nanostructures for Biomedical Applications

Laser structuring is applied to sensors for biomedical devices in versatile ways: ns-laser processing results in LIPSS for surface-enhanced Raman spectroscopy (SERS) sensors [216–219] and optically active gold nanowires [14, 220]. Furthermore, fs-laser micromachining was used for a microresonator sensor with biosensing capabilities [221] and for a stretchable sensor array for respiration monitoring [222].
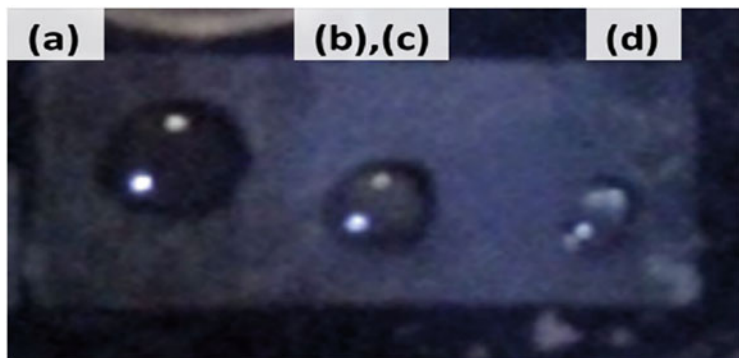
Fig. 31.22 Top-view photograph of 4 µl droplets of deionized water on steel structure taken 14 days after irradiation: (**a**) associated with spikes; (**b, c**) associated with grooves; (**d**) associated with low spatial frequency LIPSS (LSFL). The different morphologies lead to unidirectional liquid transport which is shown in the before figure. (Reprinted by permission from Springer Nature: Kirner et al. [215], Copyright (2017))
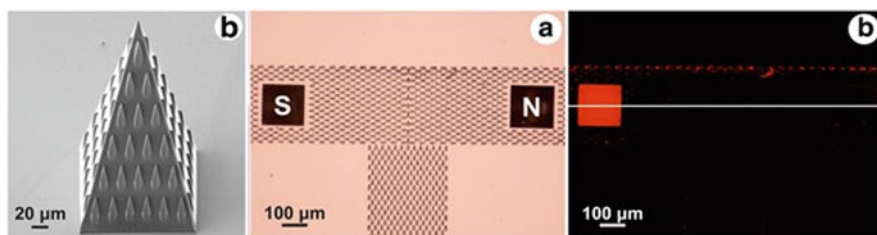

Fig. 31.23 Bio-inspired MN for efficient drug/vaccine coating. (Left) SEM image of MN. (Middle) Optical microscope image of the T-shaped channel and two microneedles after the wetting test with fluorophore solution; the one denoted with "S" is covered by bio-inspired features; the other one ("N") has plain walls. (Right) A fluorescent microscope image taken in the channel after the wetting test shows that the bio-inspired microneedle was coated significantly better with the fluorophore than the plain one. (Reprinted from Plamadeala et al. [196], which is licensed under Creative Commons Attribution 4.0 International License; http://creativecommons.org/licenses/by/4.0/)

In addition, MAPLE and the laser-induced forward transfer (LIFT) process allowed to fabricate e-noses for volatile organic compounds [223–225]. In this section, the respective works will be described in a more detailed way.

LIPSS on SU-8 polymer thin films produced by an excimer laser were sputter-coated in order to form surface plasmon polariton (SPP)-supported gold nanogratings for SERS (Figs. 31.24 and 31.25) [216, 217]. Surface-enhanced Raman spectroscopy labels have proven to be excellent for biosensing because of their merits in many aspects such as flexibility, less interference from biological matrices, high photostability, and easy multiplex encoding [218, 219]. These features make SERS labels particularly suitable for ultrasensitive detection of disease biomarkers
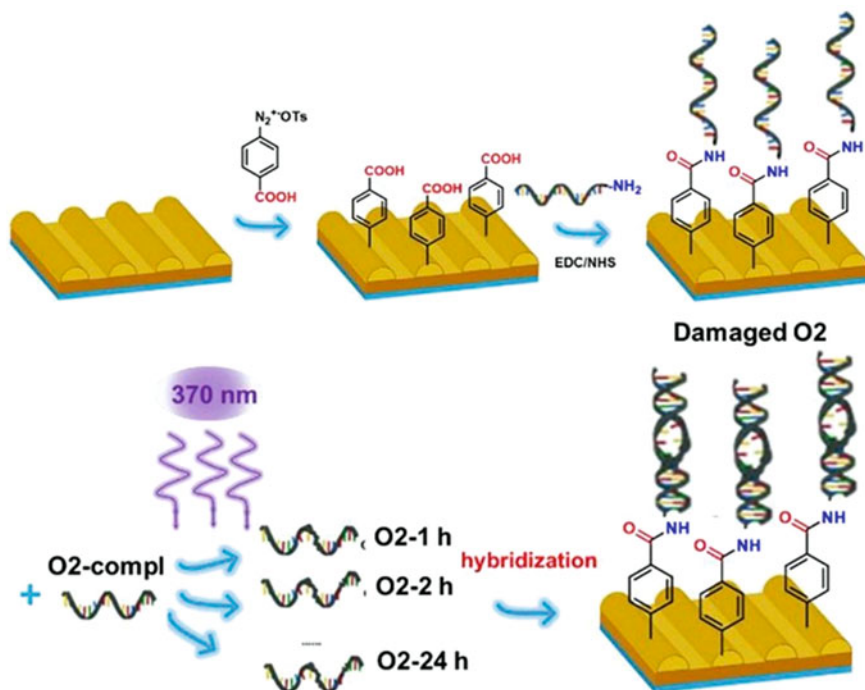
Fig. 31.24 SPP-supported gold nanogratings formed on LIPSS; the ripples were induced on polymer thin films by an excimer laser. These gratings were used for SERS. Spectra were interpreted with the help of ANN. As an explicit example, UV-induced DNA damage in oligonucleotides was detected. (Reprinted from Guselnikova et al. [217], Copyright (2019), with permission from Elsevier)

in body fluids and for targeted imaging of diseased cells and tissues, respectively [218].

Guselnikova et al. [217] combined the functional SERS sensor surface with advanced computing, namely, artificial neural networks (ANN), to collect information about the molecular structure of analytes and to evaluate spectra in the automated regime (Fig. 31.24). As an explicit example, the authors detected UV-induced DNA damage in oligonucleotide (OND) structure by the proposed method, which can be hardly measured by alternative methods [218, 219]. Erzina et al. [216] used plasmonic coupling between specific nanoparticles and underlying periodical plasmonic surface as an interdisciplinary approach for cancer detection and achieved high SERS enhancement factors (Fig. 31.25). Surface-enhanced Raman spectroscopy control spectra of normal and cancer cells' metabolites were classified by trained convolutional neural networks (CNN) and perfectly distinguished with 100% prediction accuracy. For information on other SERS applications, the reader is referred to Chap. 32.
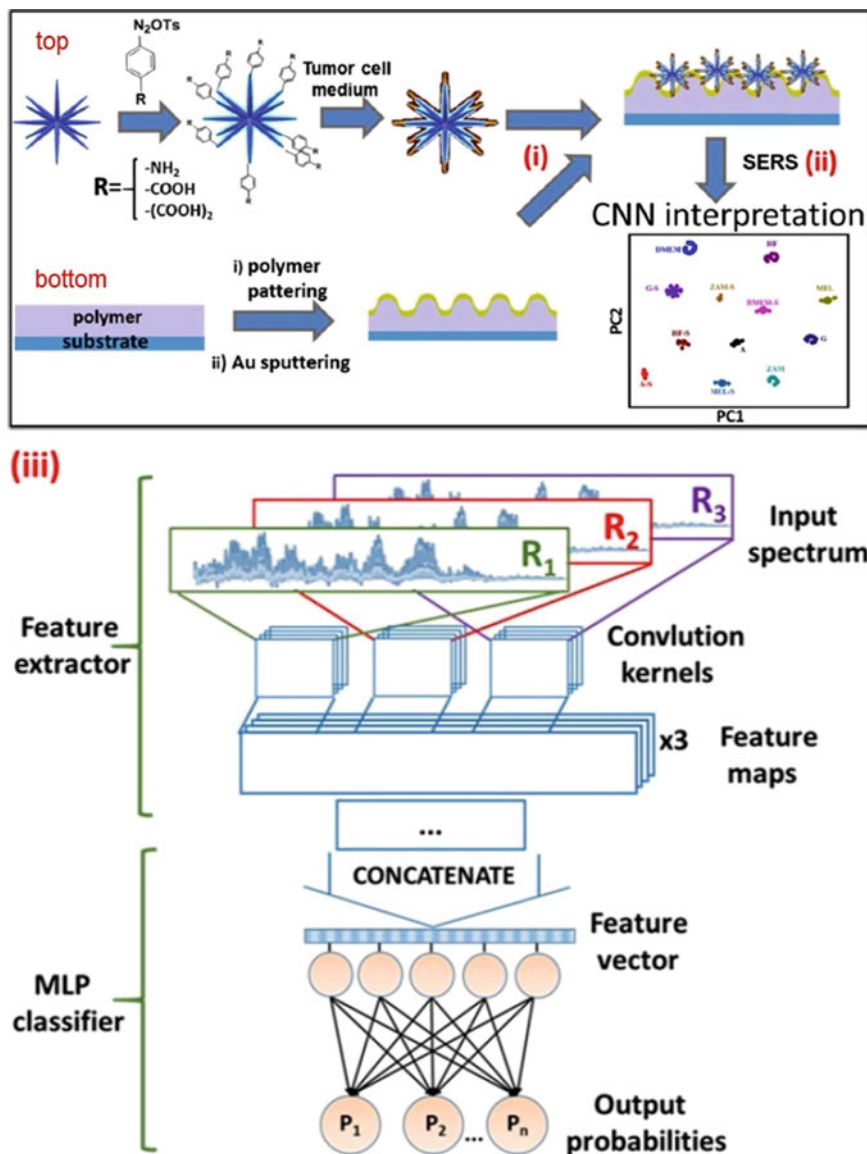
Fig. 31.25 Schematic of cancer cell detection method using nanogratings formed by an excimer laser for SERS. Top: Preparation of functional gold multibranched nanoparticles (AuMs) for interaction with tumor cells. (i) Deposition of AuMs on surface of grating. (ii) SERS measurements. Bottom: Fabrication of gold nanograting. (iii) CNN for measurement data interpretation. (Reprinted from Erzina et al. [216], Copyright (2020), with permission from Elsevier)

With a similar fabrication technique, optically active gold nanowires can be created with the help of LIPSS [14, 220, 226]. Steinhauser et al. [226] used them for localized-plasmon voltammetry which bears great potential for electrochemical sensing applications beyond conventional cyclic voltammetry. In order to determine the limitations of this method, they investigated the response toward chemical instability of the plasmonic electrode.

Kelemen et al. [221] reported on a monolithic lab-on-a-chip for label-free biosensing. To this end, they used a hybrid femtosecond laser micromachining approach combining subtractive and additive manufacturing methods. The lab-on-a-chip consists of a polymer whispering gallery mode (WGM) microresonator sensor integrated inside a glass microfluidic chip, presenting a refractive index change sensitivity of 61 nm per refractive index units (RIU). The microfluidic chips from fused silica glass were fabricated by fs-laser irradiation followed by chemical etching (FLICE) technique. A subsequent fs-laser 2PP process created WGM microresonators and coupling waveguides inside the microchannels. The biosensing capabilities of the device have been demonstrated by exploiting the biotin-streptavidin binding affinity, obtaining a measurable minimum surface density increase of 67×103 molecules per μm^2.

Koch and Dietzel [222, 227] presented a conformable sensor array to be used for triggering the artificial respiration of premature infants by measuring thorax deformations. The used sensor arrays were transferred into a stretchable format by fs-laser structuring. For the first time, signals from a stretchable sensor array are used to determine trigger points for respiration as well as for surface reconstruction taking artificial respiration to a next level.

For many years, the detection of chemical agents has been a major research topic in order to mitigate the adverse effects on environment and human health [223–225]. Benetti et al. [225] presented an e-nose for the detection of volatile compounds based on an array of six surface acoustic wave (SAW) resonators coated with five different polymers (Fig. 31.26). This e-nose is able to detect a volatile organic compound commonly used in chemical industry, namely, ethyl acetate, and simulants of chemical warfare agents, namely, dimethyl methylphosphonate (DMMP), dichloromethane (DCM), and dichloropentane (DCP). In particular, MAPLE was used to deposit thin polymer layers which were subsequently used as donor films in the laser-induced forward transfer (LIFT) process to selectively cover each SAW resonator of the array. The SAW e-nose was successfully tested upon exposure to vapors of ethyl acetate, DMMP, DCM, DCP, and water.

2.7   Other Applications

As discussed earlier, cell and bacteria behavior can be influenced by directly irradiating the interacting surface with laser light. However, lasers can also be used indirectly to achieve these effects, mainly, by the deposition of coatings onto implant materials via laser light impact. Many methods such PLD [47, 228, 229]
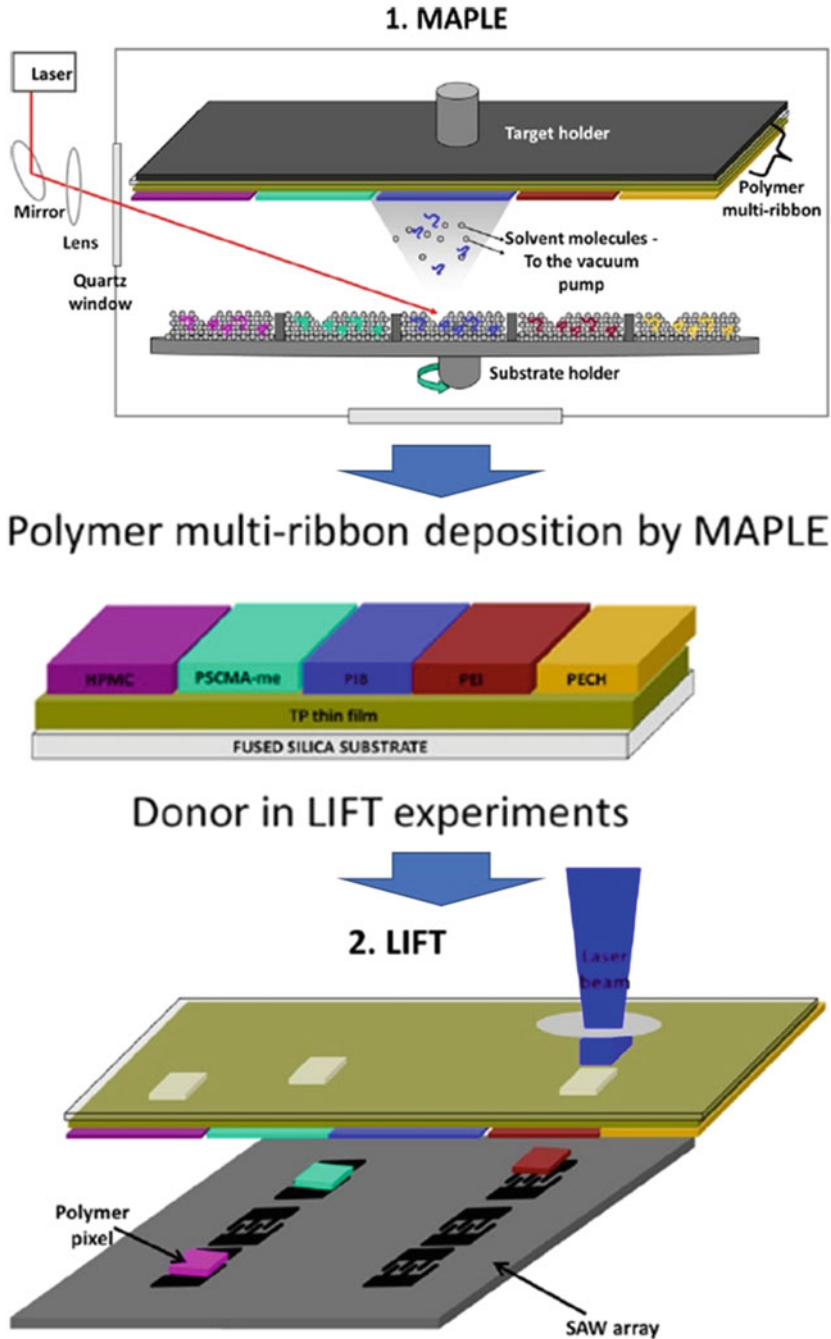
Fig. 31.26 Scheme of the laser-based methods applied for coating of the SAW devices for an e-nose for chemical agents: MAPLE is used to fabricate a polymer multi-ribbon in one step, which is afterwards used as a donor for printing of polymer pixels onto the SAW resonator by LIFT. (Reprinted from Benetti et al. [225], Copyright (2019), with permission from Elsevier)

or MAPLE [48] have been employed to achieve thin films on implant materials to render the desired surface behavior [27, 230, 231]. Metals show exceptional mechanical strength and are often used for hip replacements and dental implants [232, 233]. However, due to lack of bioactivity, metals can only function in long-term implantations after being coated with a bioactive ceramic material [234–238]. In case of enhanced osseointegration, bioactive ceramic coatings are deposited onto implant substances such as metal alloys. Especially HA coatings, belonging to the calcium phosphate group, are of high interest due to their increased performance regarding the bone-implant contact area, as bulk HA ceramics cannot be employed as implant devices due to their poor mechanical properties [239–241]. Bioactive glasses and BA+PMMA nanocomposites are also broadly used coatings on implant surfaces deposited by the PLD process [242, 243].

Laser surface structuring cannot only be used to apply coatings for biomedical uses, it can also enhance the bond strength between a medical implant and a coating, which generally leads to decreased implant failure. This principle can, for example, be employed in dentistry, where yttria-stabilized zirconia polycrystal substrates are used in dental restoration frameworks [244] and which are veneered with a feldspar-porcelain layer that should mimic the color of natural teeth for aesthetics. However, the applied ceramics are often subjected to chipping due to poor bonding to the zirconia framework, which results in high failure rates in long-term clinical use [245–247]. This problem stems from residual stresses or defects between the two layers [248–251], and this problem was found to be solved by laser structuring the zirconia surface to increase the surface roughness [252, 253] and therefore increase the bonding strength. This was compared to sandblasting, which is a standard surface treatment technique for zirconia-based dental restorations [248, 253, 254]. It was shown that laser patterning of zirconia surfaces resulted in a 75% increase in shear bond strength compared to sandblasting and an additional applied intermediate composite layer further increased the shear bond strength due to increased interlocking of the zirconia surface and veneering porcelain [255].

Besides applying coatings for biocompatibility, laser postprocessing combined with other commonly used fabrication techniques can be used to further improve the effects that are expected from a medical device. Chang et al. [256] used fs-laser post-processing combined with 3D printing to produce biodegradable poly(lactic acid) (PLA) peripheral vascular stents. These biodegradable stents give the advantage of maintaining the physiological function of natural vessels. Selective laser sintering (SLS) is a highly advantageous tool to produce complex 3D structures by computer-generated image-based design techniques [257, 258]. Mangano et al. [259] used SLS to produce titanium blade implants as a nonconventional treatment for extremely atrophied posterior mandibles. The implants showed long-term mechanical stability and good aesthetic integration. Electrosurgical blades often suffer from attachment of overheated soft tissue. To minimize the attachment, surface texturing of the blades to achieve anti-adhesive structures was investigated by Li et al. [260]. It was proposed that the laser-induced blades show hydrophobicity and therefore reduce the adhesion of soft tissue. Lasers can not only be used to structure surfaces for biomedical applications, they further can be employed directly to treat certain

diseases. Examples for fields with direct lasers treatment are ophthalmology [261, 262] and dentistry [263–265]. In Chap. 33 of this book, the authors aim to give an insight on how lasers are employed in eye disease treatment.

3 Summary and Outlook

In this chapter, the authors have presented a wide range of biomedical applications where lasers have been successfully employed to achieve a desired outcome. Tables 31.1 and 31.2 give typical examples of works which have been discussed. Lasers are a favorable tool for processing functional surfaces, as they provide the possibility of treating materials in a cost-effective and fast manner. Some laser processing methods also have the advantage of processing without contamination of the irradiated surface, which is desirable in the fields of biomedicine. The mentioned applications and effects are only possible because laser structuring provides a broad range of structure types and materials these structures can be employed on. Self-organized and directly written structures can be fabricated on materials such as metals, polymers, and composites. Metals are extensively used in implanted devices, while polymers are widely used in the field of cell scaffolds, microneedles, sensors, and analytic devices. Limits of laser structures in biomedical fields depend on the application.

While controlling cells and bacteria with laser-induced structures is possible and highly successful, one limitation is given by the fact that the processes are highly cell-dependent. In Sect. 2.1 CHO-K1 cells and HMECs show different behavior on surfaces with ripples: CHO-K1 cells align along the ripples, while HMECs do not show alignment. Instead HMECs only showed increased activation on surfaces with ripples, which was indicated by the relocation of β-catenin into the nucleus. Cell control processes are guided by micro- and nano-metric features, where nano-sized structures in the range of few nanometers interact with surface-bound proteins that guide cell adhesion processes. Self-organized structures in the range of a few nanometers have been fabricated by short wavelength systems in the EUV range, but research on these types of structures has only been conducted in the last years due to device limitations. Self-organized structures fabricated by more commonly used laser systems have sizes in the range of a few hundreds of nanometers. Requiring hierarchical multi-scale surface structuring, bacteria retention is highly favorable in the field of implanted devices.

Direct writing, for instance, TPP or laser ablation, is an important tool to fabricate cell scaffolds and microfluidic devices such as microneedles or analytic tools. Structure sizes of several hundreds of nanometers are achieved with TPP, which can be further reduced when STED is combined with TPP. With STED lithography, the lowest possible structure size is around a few tens of nanometers. This makes it possible to build cell scaffolds, where cell growth can be guided and directed with a combination of micro- and nano-sized structures. Microneedles profit from their size as minimal-invasive meddling with the body is highly desirable. Stability of the

Table 31.1 Overview on exemplary works discussed in the Sects. 2.1, 2.2, and 2.3

	Exemplary works	Authors	Material(s) and laser technique	Achievements and limits
2.1 Micro- and nanostructures for adhesion, alignment and activation of cells	Alignment of HEK-293 cells and CHO-K1 cells	Rebollar et al. [100]	LIPSS on PS by UV ns-laser (KrF excimer laser)	Alignment on ripples with periodicities > 270 nm
	Proliferation/alignment of HMECs	Schemthaner et al. [101]	LIPSS and walls on PET by UV ns-laser (KrF and ArF excimer lasers)	Proliferation increase on both structures following different mechanisms; alignment only on walls (periodicity of 1.5 microns), not on ripples (periodicity of 300 nm)
	Directing neuronal cell growth for auditory implants (pheochromocytoma cell line PC-12 and primary spiral ganglion cells)	Reich et al. [113]	Subtractive direct writing of microgrooves in silicone elastomer and platinum by fs-laser (Ti:Sapphire laser)	Guidance on neurites parallel to laser-processed grooves in platinum and grooves on molded silicone elastomer; no effect on directly laser-ablated silicone
2.2 Repellent and anti-adhesive structures for medical implants and antimicrobiotic surfaces	Repellent structures against fibroblasts for miniaturized pacemakers	Fosodeder et al. [119]	Hierarchical self-organized structures on titanium with LIPSS by fs-laser (Ti:Sapphire laser)	Expansion of the applicability of femtosecond laser processing for cell-repellence from flat samples to cylindric samples with a laser-processed ring serving as barrier for upgrowing cells
	Bacterial adhesion tested for two different test strains	Schwibbert et al. [143]	Nanostructure on PE by fs-laser (Ti:Sapphire laser)	Significant adhesion reduction of *E. coli*
	Adhesion tests of cells on different hierarchical structures ("mushrooms decorated with micro- and nanostructures")	Paun et al. [146]	2PP of IP-DIP photoresist (Nanoscribe) by fs-laser	Significant reduction of OLN-93 cell adhesion by 55%, which is an oligodendroglia cell line

2.3 Cell arrays and scaffolds for tissue engineering applications	Vascular grafts as blood vessel substitutes	Limongi et al. [162]	2PP of IP-DIP photoresist (Nanoscribe) by fs-laser	HUVECs adhere and grow on the 3D structure
	3D hydrogel cell scaffold variations (photoresist) and mechanical tests/cell growth	Yu et al. [175]	TPP of PEG-DA-based photoresists by fs-laser	High-precision configuration using 40 wt % PEG-DA and 60 wt % PE-3A (80 nm line width), optimizing mechanical stability, SH, and chitosan-assisted hydrogel for study of biocompatibility
	Retinal cell delivery scaffold variations (photoresist) and biocompatibility study	Thompson et al. [173]	TPP by fs-laser (photoresist based on acrylated poly(caprolactone):dioxane solutions)	Increasing the concentration of crosslink-able groups decreased polymerization threshold and the size of resolvable features while increasing fidelity of the scaffold; scaffold supported human retinal progenitor cells in vitro and showed favorable biocompatibility

Table 31.2 Overview on exemplary works discussed in the Sects. 2.4, 2.5, 2.6, and 2.7

	Exemplary works	Authors	Material(s) and laser technique	Achievements and limits
2.4 Microneedles for drug/vaccine delivery	Bio-inspired MN design	Plamadeala et al. [196]	TPP of OrmoComp® and OrmoComp®-based photoresists by fs-laser	Efficient (self-)coating of microneedle with drug/vaccine
	MN design variations (pore-center displacements) and penetration tests	Ovsianikov et al. [174]	TPP of Ormocer® photoresist by fs-laser	Insight in design for improved mechanical strength
	MN array design variations (needle height, shape, base width, interspacing) and insertion tests	Cordeiro et al. [192]	TPP of IPS photoresin (from Nanoscribe) by fs-laser	2PP was used for optimization of master in polymeric hydrogel MN array production
2.5 Micro- and nanostructures for fluidic systems and analysis techniques	Transwell design for MIFE	Buchroithner et al. [203]	TPP of BisSR photoresist and laser ablation of PET by fs-laser	Response of HUVECs grown on modified membranes to calcium ionophore (A23187) measured by MIFE
	Microfluidic device with micro- and nanostructures inside for vWF detection	Buchegger et al. [207]	TPP and STED lithography of PETA-based photoresists by fs-laser and continuous wave laser	Study on the impact of vWF on the activation of thrombocytes with nanoanchors of about 65 nm x 120 nm
	Tools for multi-view microscopy of single cells	Vizsnyiczai et al. [204]	TPP of SU-8 2007 photoresist by fs-laser	Significant resolution improvement by image fusion

2.6 Sensors based on micro- and nanostructures for biomedical applications	Cancer cell detection	Erzina et al. [216]	LIPSS on SU-8 photoresist by UV ns-laser (KrF excimer laser)	100% accuracy in the discrimination of tumor and normal cell's cultivation media
	Stretchable sensor for respiration monitoring	Koch and Dietzel [222, 227]	Subtractive direct writing (cutting) of polyimide foil with fs-laser	Stretchable sensor array for perfect adaption to complex 3D shapes
	e-nose for volatile organic compounds	Benetti et al. [225]	LIFT (XeCl 308 nm laser system) and MAPLE (ns-pulsed Nd:YAG laser system) of five different polymers onto substrate (fused silica with spin-coated triazene polymer)	Five volatile compounds can be detected based on SAW resonators in good agreement with theoretical sensitivities, usage at room temperature
2.7 Other applications	Biodegradable peripheral vascular stent	Chang et al. [256]	Subtractive direct writing (cutting) of PLA with fs-laser (1030 nm)	Postprocessing of 3D printed peripheral vascular stents for structural uniformity and dimensional precision, i.e., uniform structural widths, smooth edges, and accurate structural dimensions
	Surgical blade	Li et al. [260]	Self-organized surface structures on stainless steel 316L by long-pulse (μs) fiber-laser system (1070 nm)	Anti-adhesive biomimetic scales on blade for adhesion reduction of soft tissue by 16.5% on average

Table 31.3 Further development steps needed to make the methods of this chapter ready for the market

Definition of TRLs	Current status of methods from this chapter and of another exemplary chapter
TRL 1 – Basic principles observed	
TRL 2 – Technology concept formulated	
TRL 3 – Experimental proof of concept	Part of the methods from this chapter
TRL 4 – Technology validated in lab	Part of the methods from this chapter
TRL 5 – Technology validated in relevant environment (industrially relevant environment in the case of key enabling technologies)	
TRL 6 – Technology demonstrated in relevant environment (industrially relevant environment in the case of key enabling technologies)	
TRL 7 – System prototype demonstration in operational environment	
TRL 8 – System complete and qualified	
TRL 9 – Actual system proven in operational environment (competitive manufacturing in the case of key enabling technologies or in space)	Methods from Chap. 33

structure and fluid properties can limit the application of microneedles. TPP as well as DLW SM was also used in the fabrication of microfluidic channels, of analysis platforms, and of various sensors for biomedical applications. Examples of DLW SM are capillary channels capable of unidirectional liquid transport bio-inspired by spermathecae of fleas, by the integument of lizards, and by scent channels of bark bugs. Others are nanoanchors written by STED lithography which help to unravel the role of vWF in thrombocyte activation or tools written by 2PP which increase the resolution in imaging of single cells. On the other hand, also LIPSS are useful in these fields allowing the fabrication of SERS sensors which are employed for a wide range of applications such as the detection of cancer cell metabolites.

As trends in the field of biomedical applications, the authors identify the use of natural materials, laser processing of bio-inspired structures, as well as fast prototyping of personalized medical products. While other related fields presented in this book, especially the ones from Chap. 33, are used in practice with millions of treated patients, the methods presented in this chapter are in a preliminary stage. Using technology readiness levels (TRLs) (Table 31.3) as defined by the European Union[1], one would assign Chap. 33 a "TRL 9 – actual system proven in operational environment" compared to a "TRL 3 – experimental proof of concept" or "TRL 4 –

technology validated in lab" for the methods of this chapter. The largest challenge for the commercial implementation of these methods, that is, for production of medical implants or medical products with functional surfaces, is probably the fact that medical implants and products face quite strict regulations and standards and that the approval of new concepts is connected with high costs. This applies already for the achievement of "TRL 5 – technology validated in relevant environment" and "TRL 6 – technology demonstrated in relevant environment," which means in many cases animal experiments or pre-clinical studies. This challenge may be balanced by the huge market volume of the related biomedical applications and their advantages compared to the currently applied technologies. Additionally, there is a strong "technology push" by the fact that ultrafast laser systems become rapidly better, that is, more user-friendly, cheaper, and faster.

References

1. K.M. Tanvir Ahmmed, C. Grambow, A.M. Kietzig, Fabrication of micro/nano structures on metals by femtosecond laser micromachining. Micromachines **5**, 1219–1253 (2014). https://doi.org/10.3390/mi5041219
2. A. Borowiec, H.K. Haugen, Subwavelength ripple formation on the surfaces of compound semiconductors irradiated with femtosecond laser pulses. Appl. Phys. Lett. **82**, 4462–4464 (2003). https://doi.org/10.1063/1.1586457
3. J. Bonse, S. Höhm, S.V. Kirner, A. Rosenfeld, J. Krüger, Laser-induced periodic surface structures – A scientific evergreen. IEEE J. Sel. Top. Quantum Electron. **23**, 9000615 (2017). https://doi.org/10.1007/978-3-319-69537-2_17-2
4. M. Barberoglou, D. Gray, E. Magoulakis, C. Fotakis, P.A. Loukakos, E. Stratakis, Controlling ripples' periodicity using temporally delayed femtosecond laser double pulses. Opt. Express **21**, 18501 (2013). https://doi.org/10.1364/oe.21.018501
5. E. Skoulas, A. Manousaki, C. Fotakis, E. Stratakis, Biomimetic surface structuring using cylindrical vector femtosecond laser beams. Sci. Rep. **7**, 45114 (2017). https://doi.org/10.1038/srep45114
6. G.D. Tsibidis, E. Skoulas, E. Stratakis, Ripple formation on nickel irradiated with radially polarized femtosecond beams. Opt. Lett. **40**, 5172 (2015). https://doi.org/10.1364/ol.40.005172
7. O.J. Allegre, W. Perrie, S.P. Edwardson, G. Dearden, K.G. Watkins, Laser microprocessing of steel with radially and azimuthally polarized femtosecond vortex pulses. J. Opt. (U. K.) **14**, 085601 (2012). https://doi.org/10.1088/2040-8978/14/8/085601
8. O.J. Allegre, Y. Jin, W. Perrie, J. Ouyang, E. Fearon, S.P. Edwardson, G. Dearden, Complete wavefront and polarization control for ultrashort-pulse laser microprocessing. Opt. Express **21**, 21198 (2013). https://doi.org/10.1364/oe.21.021198
9. J.M. Romano, R. Helbig, F. Fraggelakis, A. Garcia-Giron, C. Werner, R. Kling, S. Dimov, Springtail-inspired triangular laser-induced surface textures on metals using MHz ultrashort pulses. J. Micro Nano-Manuf. **7**, 024504 (2019). https://doi.org/10.1115/1.4043417

10. J.M. Romano, A. Garcia-Giron, P. Penchev, S. Dimov, Triangular laser-induced submicron textures for functionalising stainless steel surfaces. Appl. Surf. Sci. **440**, 162–169 (2018). https://doi.org/10.1016/j.apsusc.2018.01.086

11. U. Hermens, S.V. Kirner, C. Emonts, P. Comanns, E. Skoulas, A. Mimidis, H. Mescheder, K. Winands, J. Krüger, E. Stratakis, J. Bonse, Mimicking lizard-like surface structures upon ultrashort laser pulse irradiation of inorganic materials. Appl. Surf. Sci. **418**, 499–507 (2017). https://doi.org/10.1016/j.apsusc.2016.12.112

12. Y. Liu, S. Li, S. Niu, X. Cao, Z. Han, L. Ren, Bio-inspired micro-nano structured surface with structural color and anisotropic wettability on Cu substrate. Appl. Surf. Sci. **379**, 230–237 (2016). https://doi.org/10.1016/j.apsusc.2016.03.234

13. E. Rebollar, M. Castillejo, T.A. Ezquerra, Laser induced periodic surface structures on polymer films: From fundamentals to applications. Eur. Polym. J. **73**, 162–174 (2015). https://doi.org/10.1016/j.eurpolymj.2015.10.012

14. R.A. Barb, C. Hrelescu, L. Dong, J. Heitz, J. Siegel, P. Slepicka, V. Vosmanska, V. Svorcik, B. Magnus, R. Marksteiner, M. Schernthaner, K. Groschner, Laser-induced periodic surface structures on polymers for formation of gold nanowires and activation of human cells. Appl. Phys. A Mater. Sci. Process. **117**, 295–300 (2014). https://doi.org/10.1007/s00339-013-8219-9

15. J. Heitz, B. Reisinger, S. Yakunin, N. Voelcker, Q. Peng, A.L. Hook, C. Romanin, M. Fahrner, Laser-induced micro- and nanostructures at polymer surfaces for applications in cell biology, in *Int. Conf. Transparent Opt. Networks*, (2011), pp. 2–5. https://doi.org/10.1109/ICTON.2011.5970989

16. J. Heitz, B. Reisinger, M. Fahrner, C. Romanin, J. Siegel, V. Svorcik, Laser-induced periodic surface structures (LIPSS) on polymer, in *2012 14th Int. Conf. Transparent Opt. Networks*, (2012), pp. 1–4. https://doi.org/10.1109/ICTON.2012.6253723

17. S. Höhm, A. Rosenfeld, J. Krüger, J. Bonse, Femtosecond diffraction dynamics of laser-induced periodic surface structures on fused silica. Appl. Phys. Lett. **102**, 054102 (2013). https://doi.org/10.1063/1.4790284

18. B.K. Nayak, M.C. Gupta, Ultrafast laser-induced self-organized conical micro/nano surface structures and their origin. Opt. Lasers Eng. **48**, 966–973 (2010). https://doi.org/10.1016/j.optlaseng.2010.05.009

19. D. Dufft, A. Rosenfeld, S.K. Das, R. Grunwald, J. Bonse, Femtosecond laser-induced periodic surface structures revisited: A comparative study on ZnO. J. Appl. Phys. **105**, 034908 (2009). https://doi.org/10.1063/1.3074106

20. V. Zorba, E. Stratakis, M. Barberoglou, E. Spanakis, P. Tzanetakis, S.H. Anastasiadis, C. Fotakis, Biomimetic artificial surfaces quantitatively reproduce the water repellency of a lotus leaf. Adv. Mater. **20**, 4049–4054 (2008). https://doi.org/10.1002/adma.200800651

21. T.H. Her, R.J. Finlay, C. Wu, S. Deliwala, E. Mazur, Microstructuring of silicon with femtosecond laser pulses. Appl. Phys. Lett. **73**, 1673–1675 (1998). https://doi.org/10.1063/1.122241

22. X. Wang, C. Li, W. Hong, C. Ma, Y. Xing, J. Feng, Fabrication of ordered hierarchical structures on stainless steel by picosecond laser for modified wettability applications. Opt. Express **26**, 18998 (2018). https://doi.org/10.1364/oe.26.018998

23. M. Martínez-Calderon, A. Rodríguez, A. Dias-Ponte, M.C. Morant-Miñana, M. Gómez-Aranzadi, S.M. Olaizola, Femtosecond laser fabrication of highly hydrophobic stainless steel surface with hierarchical structures fabricated by combining ordered microstructures and LIPSS. Appl. Surf. Sci. **374**, 81–89 (2016). https://doi.org/10.1016/j.apsusc.2015.09.261

24. D.W. Bäuerle, *Laser Processing and Chemistry* (Springer, Berlin Heidelberg, 2011)

25. J. Heitz, C. Plamadeala, M. Muck, O. Armbruster, W. Baumgartner, A. Weth, C. Steinwender, H. Blessberger, J. Kellermair, S.V. Kirner, J. Krüger, J. Bonse, A.S. Guntner, A.W. Hassel, Femtosecond laser-induced microstructures on Ti substrates for reduced cell adhesion. Appl. Phys. A Mater. Sci. Process. **123**, 734 (2017). https://doi.org/10.1007/s00339-017-1352-0

26. A.Y. Vorobyev, C. Guo, Femtosecond laser structuring of titanium implants. Appl. Surf. Sci. **253**, 7272–7280 (2007). https://doi.org/10.1016/j.apsusc.2007.03.006

27. P. Shukla, D.G. Waugh, J. Lawrence, R. Vilar, Laser surface structuring of ceramics, metals and polymers for biomedical applications: A review, in *Laser Surface Modification of Biomaterials: Techniques and Applications*, (Elsevier Ltd, San Diego, 2016), pp. 281–299

28. A. Riveiro, A.L.B. Maçon, J. del Val, R. Comesaña, J. Pou, Laser surface texturing of polymers for biomedical applications. Front. Phys. **6**, 16 (2018). https://doi.org/10.3389/fphy.2018.00016

29. A.Y. Fasasi, S. Mwenifumbo, N. Rahbar, J. Chen, M. Li, A.C. Beye, C.B. Arnold, W.O. Soboyejo, Nano-second UV laser processed micro-grooves on Ti6Al4V for biomedical applications. Mater. Sci. Eng. C **29**, 5–13 (2009). https://doi.org/10.1016/j.msec.2008.05.002

30. M.P. Fiorucci, A.J. López, A. Ramil, Surface modification of Ti6Al4V by nanosecond laser ablation for biomedical applications. J. Phys. Conf. Ser. **605**, 012022 (2015). https://doi.org/10.1088/1742-6596/605/1/012022

31. E. Stratakis, J. Bonse, J. Heitz, J. Siegel, G.D. Tsibidis, E. Skoulas, A. Papadopoulos, A. Mimidis, A.C. Joel, P. Comanns, J. Krüger, C. Florian, Y. Fuentes-Edfuf, J. Solis, W. Baumgartner, Laser engineering of biomimetic surfaces. Mater. Sci. Eng. R Rep. **141**, 100562 (2020). https://doi.org/10.1016/j.mser.2020.100562

32. J. Stampfl, R. Liska, A. Ovsianikov, *Multiphoton Lithography* (Wiley-VCH Verlag GmbH & Co., Weinheim, Germany, 2016)

33. S. Maruo, O. Nakamura, S. Kawata, Three-dimensional microfabrication with two-photon-absorbed photopolymerization. Opt. Lett. **22**, 132–134 (1997)

34. K. König, A. Ostendorf, *Optically Induced Nanostructures: Biomedical and Technical Applications* (De Gruyter, Berlin, 2015)

35. C. Liao, A. Wuethrich, M. Trau, A material odyssey for 3D nano/microstructures: Two photon polymerization based nanolithography in bioapplications. Appl. Mater. Today **19**, 100635 (2020). https://doi.org/10.1016/j.apmt.2020.100635

36. T. Baldacchini, *Three-Dimensional Microfabrication Using Two-Photon Polymerization: Fundamentals, Technology, and Applications* (William Andrew, Oxford, UK, 2015)

37. X. Wang, Z. Wei, C.Z. Baysah, M. Zheng, J. Xing, Biomaterial-based microstructures fabricated by two-photon polymerization microfabrication technology. RSC Adv. **9**, 34472–34480 (2019). https://doi.org/10.1039/c9ra05645a

38. G. Weisgrab, O. Guillaume, Z. Guo, P. Heimel, P. Slezak, A. Poot, D. Grijpma, A. Ovsianikov, 3D printing of large-scale and highly porous biodegradable tissue engineering scaffolds from poly(trimethylene-carbonate) using two-photon-polymerization. Biofabrication **12**, 045036 (2020). https://doi.org/10.1088/1758-5090/abb539

39. A. Daskalova, L. Angelova, A. Carvalho, A. Trifonov, C. Nathala, F. Monteiro, I. Buchvarov, Effect of surface modification by femtosecond laser on zirconia based ceramics for screening of cell-surface interaction. Appl. Surf. Sci. **513**, 145914 (2020). https://doi.org/10.1016/j.apsusc.2020.145914

40. S. Marimuthu, S. Pathak, J. Radhakrishnan, A.M. Kamara, In-process monitoring of laser surface modification. Coatings **11**, 886 (2021). https://doi.org/10.3390/coatings11080886

41. Z.C. Chen, T.L. Chang, C.C. Liu, W.T. Hsiao, C.H. Huang, Picosecond laser surface modification of aluminum oxide with fish-scale structures for cell culture. Ceram. Int. **46**, 17651–17658 (2020). https://doi.org/10.1016/j.ceramint.2020.04.067

42. A.K. Nath, Chapter 9.06 - laser Drilling of Metallic and Nonmetallic Substrates, in *Comprehensive Materials Processing*, ed. by S. Hashmi, G. F. Batalha, C. J. Van Tyne, B. Yilbas, (Elsevier Ltd., New York, USA, 2014), pp. 115–175. https://doi.org/10.1016/B978-0-08-096532-1.00904-3

43. I. Miyamoto, H. Maruo, Mechanism of laser cutting. Weld. World, Le Soudage Dans Le Monde **29**, 283–294 (1991). https://doi.org/10.22486/iwj.v25i2.148338

44. I. Miyamoto, K. Cvecek, M. Schmidt, Advances of laser welding technology of glass - science and technology. J. Laser Micro Nanoeng. **15**, 63–76 (2020). https://doi.org/10.2961/jlmn.2020.02.1001

45. M. Malinauskas, L. Lukoševičius, D. Mackevičiūtė, E. Balčiūnas, S. Rekštytė, D. Paipulas, Multiscale 3D manufacturing: Combining thermal extrusion printing with additive and

subtractive direct laser writing. Laser Sources Appl. II **9135**, 91350T (2014). https://doi.org/10.1117/12.2051520

46. L. D'Alessio, R. Teghil, M. Zaccagnino, I. Zaccardo, D. Ferro, V. Marotta, Pulsed laser ablation and deposition of bioactive glass as coating material for biomedical applications. Appl. Surf. Sci. **138–139**, 527–532 (1999). https://doi.org/10.1016/S0169-4332(98)00610-2

47. H.-U. Krebs, M. Weisheit, J. Faupel, E. Süske, T. Scharf, C. Fuhse, M. Störmer, K. Sturm, M. Seibt, H. Kijewski, D. Nelke, E. Panchenko, M. Buback, Pulsed laser deposition (PLD)-a versatile thin film technique, in *Advances in Solid State Physics*, (Springer, Berlin, Heidelberg, 2003), pp. 505–518

48. A. Piqué, The matrix-assisted pulsed laser evaporation (MAPLE) process: Origins and future directions. Appl. Phys. A Mater. Sci. Process. **105**, 517–528 (2011). https://doi.org/10.1007/s00339-011-6594-7

49. A. Bigi, B. Bracci, F. Cuisinier, R. Elkaim, M. Fini, I. Mayer, I.N. Mihailescu, G. Socol, L. Sturba, P. Torricelli, Human osteoblast response to pulsed laser deposited calcium phosphate coatings. Biomaterials **26**, 2381–2389 (2005). https://doi.org/10.1016/j.biomaterials.2004.07.057

50. I.N. Zavestovskaya, Laser nanostructuring of materials surfaces. Quantum Electron. **40**, 942–954 (2010). https://doi.org/10.1070/qe2010v040n11abeh014447

51. A. Kurella, N.B. Dahotre, Review paper: Surface modification for bioimplants: The role of laser surface engineering. J. Biomater. Appl. **20**, 5–50 (2005). https://doi.org/10.1177/0885328205052974

52. C.F. Koch, S. Johnson, D. Kumar, M. Jelinek, D.B. Chrisey, A. Doraiswamy, C. Jin, R.J. Narayan, I.N. Mihailescu, Pulsed laser deposition of hydroxyapatite thin films. Mater. Sci. Eng. C **27**, 484–494 (2007). https://doi.org/10.1016/j.msec.2006.05.025

53. A. Piqué, D.B. Chrisey, B.J. Spargo, M.A. Bucaro, R.W. Vachet, J.H. Callahan, R.A. McGill, D. Leonhardt, T.E. Mlsna, Use of matrix assisted pulsed laser evaporation (MAPLE) for the growth of organic thin films. MRS Online Proc. Libr. Arch. **526**, 421–426 (1998). https://doi.org/10.1557/PROC-526-421

54. K.B. Shepard, R.D. Priestley, MAPLE deposition of macromolecules. Macromol. Chem. Phys. **214**, 862–872 (2013). https://doi.org/10.1002/macp.201200621

55. F. Sima, P. Davidson, E. Pauthe, L.E. Sima, O. Gallet, I.N. Mihailescu, K. Anselme, Fibronectin layers by matrix-assisted pulsed laser evaporation from saline buffer-based cryogenic targets. Acta Biomater. **7**, 3780–3788 (2011). https://doi.org/10.1016/j.actbio.2011.06.016

56. C. Constantinescu, A. Palla-Papavlu, A. Rotaru, P. Florian, F. Chelu, M. Icriverzi, A. Nedelcea, V. Dinca, A. Roseanu, M. Dinescu, Multifunctional thin films of lactoferrin for biochemical use deposited by MAPLE technique. Appl. Surf. Sci. **255**, 5491–5495 (2009). https://doi.org/10.1016/j.apsusc.2008.07.163

57. I.A. Paun, A. Moldovan, C.R. Luculescu, M. Dinescu, Biocompatible polymeric implants for controlled drug delivery produced by MAPLE. Appl. Surf. Sci. **257**, 10780–10788 (2011). https://doi.org/10.1016/j.apsusc.2011.07.097

58. V. Dinca, C. Viespe, S. Brajnicov, I. Constantinoiu, A. Moldovan, A. Bonciu, C.N. Toader, R.E. Ginghina, N. Grigoriu, M. Dinescu, N.D. Scarisoreanu, MAPLE assembled acetylcholinesterase– Polyethylenimine hybrid and multilayered interfaces for toxic gases detection. Sensors (Switzerland) **18**, 4265 (2018). https://doi.org/10.3390/s18124265

59. I.A. Paun, A.M. Acasandrei, C.R. Luculescu, C.C. Mustaciosu, V. Ion, M. Mihailescu, E. Vasile, M. Dinescu, MAPLE deposition of polypyrrole-based composite layers for bone regeneration. Appl. Surf. Sci. **357**, 975–984 (2015). https://doi.org/10.1016/j.apsusc.2015.09.083

60. A. Pérez Del Pino, P. Serra, J.L. Morenza, Oxidation of titanium through Nd:YAG laser irradiation. Appl. Surf. Sci. 197–198, 887–890 (2002). https://doi.org/10.1016/S0169-4332(02)00447-6

61. M.T. Mohammed, Z.A. Khan, A.N. Siddiquee, Surface modifications of titanium materials for developing corrosion behavior in human body environment: A review. Procedia Mater. Sci. **6**, 1610–1618 (2014). https://doi.org/10.1016/j.mspro.2014.07.144

62. F.J.C. Braga, R.F.C. Marques, E.d.A. Filho, A.C. Guastaldi, Surface modification of Ti dental implants by Nd:YVO 4 laser irradiation. Appl. Surf. Sci. **253**, 9203–9208 (2007). https://doi.org/10.1016/j.apsusc.2007.05.048

63. S.A. Lone, M. Muck, P. Fosodeder, C.C. Mardare, C. Florian, A. Weth, J. Krüger, C. Steinwender, W. Baumgartner, J. Bonse, J. Heitz, A.W. Hassel, Impact of femtosecond laser treatment accompanied with anodization of titanium alloy on fibroblast cell growth. Phys. Status Solidi Appl. Mater. Sci. **217**, 1900838 (2020). https://doi.org/10.1002/pssa.201900838

64. M.V. Diamanti, B. del Curto, M. Pedeferri, Anodic oxidation of titanium: From technical aspects to biomedical applications. J. Appl. Biomater. Biomech. **9**, 55–69 (2011). https://doi.org/10.5301/JABB.2011.7429

65. O. Nedela, P. Slepicka, V. Švorcík, Surface modification of polymer substrates for biomedical applications. Materials (Basel). **10**, 1115 (2017). https://doi.org/10.3390/ma10101115

66. T. Gumpenberger, J. Heitz, D. Bäuerle, H. Kahr, I. Graz, C. Romanin, V. Svorcik, F. Leisch, Adhesion and proliferation of human endothelial cells on photochemically modified polytetrafluoroethylene. Biomaterials **24**, 5139–5144 (2003). https://doi.org/10.1016/S0142-9612(03)00460-5

67. J. Heitz, M. Olbrich, S. Moritz, C. Romanin, V. Svorcik, D. Bäuerle, Surface modification of polmers by UV-irradition: Applications in micro-and biotechnology. Lasers Appl. **59581U** (2005). https://doi.org/10.1117/12.620816

68. H. Watanabe, T. Takata, M. Tsuge, Polymer surface modification due to excimer laser radiation—Chemical and physical changes in the surface structure of poly(ethylene terephthalate). Polym. Int. **31**, 247–254 (1993). https://doi.org/10.1002/pi.4990310306

69. W. Wong, K. Chan, K.W. Yeung, K.S. Lau, Chemical surface modification of poly (ethylene terephthalate) by excimer irradiation of high and low intensities. Mater. Res. Innov. **4**, 344–349 (2001). https://doi.org/10.1007/s100190000116

70. A.M. Richter, G. Buchberger, D. Stifter, J. Duchoslav, A. Hertwig, J. Bonse, J. Heitz, K. Schwibbert, Spatial period of laser-induced surface nanoripples on PET determines Escherichia coli repellence. Nanomaterials **11**, 3000 (2021). https://doi.org/10.3390/nano11113000

71. J. Heitz, M. Muck, J. Vujovic, W. Baumgartner, A.W. Hassel, S.A. Lone, B. Steinhauser, C. Hrelescu, T.A. Klar, G. Buchberger, A. Weth, D. Baiko, Laser-induced periodic surface structures (LIPSS) for biomedical and sensing applications, in *Int. Conf. Transparent Opt. Networks*, 8–11 July 2020 (2020). https://doi.org/10.1109/ICTON51198.2020.9203402

72. A. Ranella, M. Barberoglou, S. Bakogianni, C. Fotakis, E. Stratakis, Tuning cell adhesion by controlling the roughness and wettability of 3D micro/nano silicon structures. Acta Biomater. **6**, 2711–2720 (2010). https://doi.org/10.1016/j.actbio.2010.01.016

73. S. Yakunin, M. Fahrner, B. Reisinger, H. Itani, C. Romanin, J. Heitz, Laser microstructuring of photomodified fluorinated ethylene propylene surface for confined growth of Chinese hamster ovary cells and single cell isolation. J. Biomed. Mater. Res. – Part B Appl. Biomater. **100**, 170–176 (2012). https://doi.org/10.1002/jbm.b.31935

74. S. Schlie, E. Fadeeva, J. Koch, A. Ngezahayo, B.N. Chichkov, Femtosecond laser fabricated spike structures for selective control of cellular behavior. J. Biomater. Appl. **25**, 217–233 (2010). https://doi.org/10.1177/0885328209345553

75. A.I. Teixeira, P.F. Nealey, C.J. Murphy, Responses of human keratocytes to micro- and nanostructured substrates. J. Biomed. Mater. Res. – Part A **71**, 369–376 (2004). https://doi.org/10.1002/jbm.a.30089

76. C. Xu, F. Yang, S. Wang, S. Ramakrishna, In vitro study of human vascular endothelial cell function on materials with various surface roughness. J. Biomed. Mater. Res. – Part A **71**, 154–161 (2004). https://doi.org/10.1002/jbm.a.30143

77. C.S. Ranucci, P.V. Moghe, Substrate microtopography can enhance cell adhesive and migratory responsiveness to matrix ligand density. J. Biomed. Mater. Res. **54**, 149–161 (2001). https://doi.org/10.1002/1097-4636(200102)54:2<149::AID-JBM1>3.0.CO;2-O

78. Y. Wan, Y. Wang, Z. Liu, X. Qu, B. Han, J. Bei, S. Wang, Adhesion and proliferation of OCT-1 osteoblast-like cells on micro- and nano-scale topography structured poly(L-lactide). Biomaterials **26**, 4453–4459 (2005). https://doi.org/10.1016/j.biomaterials.2004.11.016

79. A.I. Teixeira, G.A. McKie, J.D. Foley, P.J. Bertics, P.F. Nealey, C.J. Murphy, The effect of environmental factors on the response of human corneal epithelial cells to nanoscale substrate topography. Biomaterials **27**, 3945–3954 (2006). https://doi.org/10.1016/j.biomaterials.2006.01.044

80. A.C. Duncan, F. Rouais, S. Lazare, L. Bordenave, C. Baquey, Effect of laser modified surface microtopochemistry on endothelial cell growth. Colloids Surf. B Biointerfaces **54**, 150–159 (2007). https://doi.org/10.1016/j.colsurfb.2006.09.013

81. M. Arnold, E.A. Cavalcanti-Adam, R. Glass, J. Blümmel, W. Eck, M. Kantlehner, H. Kessler, J.P. Spatz, Activation of integrin function by nanopatterned adhesive interfaces. ChemPhysChem **5**, 383–388 (2004). https://doi.org/10.1002/cphc.200301014

82. A. Thapa, T.J. Webster, K.M. Haberstroh, Polymers with nano-dimensional surface features enhance bladder smooth muscle cell adhesion. J. Biomed. Mater. Res. – Part A **67**, 1374–1383 (2003). https://doi.org/10.1002/jbm.a.20037

83. D.J.S. Hulmes, Building collagen molecules, fibrils, and suprafibrillar structures. J. Struct. Biol. **137**, 2–10 (2002). https://doi.org/10.1006/jsbi.2002.4450

84. K. Anselme, Osteoblast adhesion on biomaterials. Biomaterials **21**, 667–681 (2000). https://doi.org/10.1016/S0142-9612(99)00242-2

85. B. Kasemo, Biological surface science. Surf. Sci. **500**, 656–677 (2002)

86. D.A. Puleo, A. Nanci, Understanding and controlling the bone-implant interface. Biomaterials **20**, 2311–2321 (1999)

87. C.J. Wilson, R.E. Clegg, D.I. Leavesley, M.J. Pearcy, Mediation of biomaterial-cell interactions by adsorbed proteins: A review. Tissue Eng. **11**, 1–18 (2005). https://doi.org/10.1089/ten.2005.11.1

88. P. Roach, D. Eglin, K. Rohde, C.C. Perry, Modern biomaterials: A review – Bulk properties and implications of surface modifications. J. Mater. Sci. Mater. Med. **18**, 1263–1277 (2007). https://doi.org/10.1007/s10856-006-0064-3

89. B. Kasemo, J. Gold, Implant surfaces and interface processes. Adv. Dent. Res. **13**, 8–20 (1999). https://doi.org/10.1177/08959374990130011901

90. K. Rechendorff, M.B. Hovgaard, M. Foss, V.P. Zhdanov, F. Besenbacher, Enhancement of protein adsorption induced by surface roughness. Langmuir **22**, 10885–10888 (2006). https://doi.org/10.1021/la0621923

91. M.B. Hovgaard, K. Rechendorff, J. Chevallier, M. Foss, F. Besenbacher, Fibronectin adsorption on tantalum: The influence of nanoroughness. J. Phys. Chem. B **112**, 8241–8249 (2008). https://doi.org/10.1021/jp801103n

92. F.A. Denis, P. Hanarp, D.S. Sutherland, J. Gold, C. Mustin, P.G. Rouxhet, Y.F. Dufrêne, Protein adsorption on model surfaces with controlled nanotopography and chemistry. Langmuir **18**, 819–828 (2002). https://doi.org/10.1021/la011011o

93. L. Richert, F. Variola, F. Rosei, J.D. Wuest, A. Nanci, Adsorption of proteins on nanoporous Ti surfaces. Surf. Sci. **604**, 1445–1451 (2010). https://doi.org/10.1016/j.susc.2010.05.007

94. T. Peterbauer, S. Yakunin, J. Siegel, S. Hering, M. Fahrner, C. Romanin, J. Heitz, Dynamics of spreading and alignment of cells cultured in vitro on a grooved polymer surface. J. Nanomater. **2011**, 413079 (2011). https://doi.org/10.1155/2011/413079

95. B. Zhu, Q. Lu, J. Yin, J. Hu, Z. Wang, Effects of laser-modified polystyrene substrate on CHO cell growth and alignment. J. Biomed. Mater. Res. – Part B Appl. Biomater. **70**, 43–48 (2004). https://doi.org/10.1002/jbm.b.30011

96. W. Xuefeng, C. André Ohlin, Q. Lu, J. Hu, Influence of physicochemical properties of laser-modified polystyrene on bovine serum albumin adsorption and rat C6 glioma cell behavior. J. Biomed. Mater. Res. Part A **79**, 963–973 (2006). https://doi.org/10.1002/jbm.a

97. B. Zhu, Q. Zhang, Q. Lu, Y. Xu, J. Yin, J. Hu, Z. Wang, Nanotopographical guidance of C6 glioma cell alignment and oriented growth. Biomaterials **25**, 4215–4223 (2004). https://doi.org/10.1016/j.biomaterials.2003.11.020

98. E. Arenholz, J. Heitz, M. Himmelbauer, D. Bäuerle, Laser-enhanced adhesion and thin film formation, in *ALT'95 International Symposium on Advanced Materials for Optics and Optoelectronics*, (1996), pp. 90–97

99. S. Lazare, P. Benet, Surface amorphization of Mylar(R) films with the excimer laser radiation above and below ablation threshold: Ellipsometric measurements. J. Appl. Phys. **74**, 4953–4957 (1993). https://doi.org/10.1063/1.354333

100. E. Rebollar, I. Frischauf, M. Olbrich, T. Peterbauer, S. Hering, J. Preiner, P. Hinterdorfer, C. Romanin, J. Heitz, Proliferation of aligned mammalian cells on laser-nanostructured polystyrene. Biomaterials **29**, 1796–1806 (2008). https://doi.org/10.1016/j.biomaterials.2007.12.039

101. M. Schernthaner, B. Reisinger, H. Wolinski, S.D. Kohlwein, A. Trantina-Yates, M. Fahrner, C. Romanin, H. Itani, D. Stifter, G. Leitinger, K. Groschner, J. Heitz, Nanopatterned polymer substrates promote endothelial proliferation by initiation of β-catenin transcriptional signaling. Acta Biomater. **8**, 2953–2962 (2012). https://doi.org/10.1016/j.actbio.2012.04.018

102. B.T. MacDonald, K. Tamai, X. He, Wnt/β-catenin signaling: Components, mechanisms, and diseases. Dev. Cell **17**, 9–26 (2009). https://doi.org/10.1016/j.devcel.2009.06.016

103. T.P. Rao, M. Kühl, An updated overview on wnt signaling pathways: A prelude for more. Circ. Res. **106**, 1798–1806 (2010). https://doi.org/10.1161/CIRCRESAHA.110.219840

104. M. Schernthaner, G. Leitinger, H. Wolinski, S.D. Kohlwein, B. Reisinger, R.A. Barb, W.F. Graier, J. Heitz, K. Groschner, Enhanced Ca2+ entry and tyrosine phosphorylation mediate nanostructure-induced endothelial proliferation. J. Nanomater. **2013**, 251063 (2013). https://doi.org/10.1155/2013/251063

105. B. Reisinger, M. Fahrner, I. Frischauf, S. Yakunin, V. Svorcik, H. Fiedorowicz, A. Bartnik, C. Romanin, J. Heitz, EUV micropatterning for biocompatibility control of PET. Appl. Phys. A: Mater. Sci. Process. **100**, 511–516 (2010). https://doi.org/10.1007/s00339-010-5845-3

106. A. Bartnik, H. Fiedorowicz, R. Jarocki, J. Kostecki, A. Szczurek, M. Szczurek, Ablation and surface modifications of PMMA using a laser-plasma EUV source. Appl. Phys. B Lasers Opt. **96**, 727–730 (2009). https://doi.org/10.1007/s00340-009-3692-8

107. A. Bartnik, H. Fiedorowicz, R. Jarocki, J. Kostecki, R. Rakowski, A. Szczurek, M. Szczurek, Micro-and nanoprocessing of polymers using a laser plasma extreme ultraviolet source. Acta Phys. Pol. A. **117**, 384–390 (2010). https://doi.org/10.12693/APhysPolA.117.384

108. M.N. Calmels, I. Saliba, G. Wanna, N. Cochard, J. Fillaux, O. Deguine, B. Fraysse, Speech perception and speech intelligibility in children after cochlear implantation. Int. J. Pediatr. Otorhinolaryngol. **68**, 347–351 (2004). https://doi.org/10.1016/j.ijporl.2003.11.006

109. J. Murphy, G. O'Donoghue, Bilateral cochlear implantation: An evidence-based medicine evaluation. Laryngoscope **117**, 1412–1418 (2007). https://doi.org/10.1097/MLG.0b013e318068b594

110. S.C. Peng, J.B. Tomblin, C.W. Turner, Production and perception of speech intonation in pediatric cochlear implant recipients and individuals with normal hearing. Ear Hear. **29**, 336–351 (2008). https://doi.org/10.1097/AUD.0b013e318168d94d

111. J. Xu, R.K. Shepherd, R.E. Millard, G.M. Clark, Chronic electrical stimulation of the auditory nerve at high stimulus rates: A physiological and histopathological study. Hear. Res. **105**, 1–29 (1997). https://doi.org/10.1016/S0378-5955(96)00193-1

112. C. Newbold, R. Richardson, R. Millard, C. Huang, D. Milojevic, R. Shepherd, R. Cowan, Changes in biphasic electrode impedance with protein adsorption and cell growth. J. Neural Eng. **7**, 056011 (2010). https://doi.org/10.1088/1741-2560/7/5/056011

113. U. Reich, E. Fadeeva, A. Warnecke, G. Paasche, P. Müller, B. Chichkov, T. Stöver, T. Lenarz, G. Reuter, Directing neuronal cell growth on implant material surfaces by microstructuring. J. Biomed. Mater. Res. – Part B Appl. Biomater. **100**(B), 940–947 (2012). https://doi.org/10.1002/jbm.b.32656

114. A. Klos, X. Sedao, T.E. Itina, C. Helfenstein-Didier, C. Donnet, S. Peyroche, L. Vico, A. Guignandon, V. Dumas, Ultrafast laser processing of nanostructured patterns for the control of cell adhesion and migration on titanium alloy. Nanomaterials **10**, 864 (2020). https://doi.org/10.3390/nano10050864

115. C. Steinwender, S. Hönig, K. Salch, J. Kammler, H. Blessberger, S. Schwarz, A. Nahler, V. Gammer, M. Grund, A. Kypta, First-in-man experience with a minimally invasive transcatheter pacemaker. Wien. Klin. Wochenschr. **126**, 78 (2014)

116. M. Muck, B. Wolfsjäger, K. Seibert, C. Maier, S.A. Lone, A.W. Hassel, W. Baumgart-ner, J. Heitz, Femtosecond laser-processing of pre-anodized Ti-based bone implants for cell-repellent functionalization. Nanomaterials **11**, 1342 (2021). https://doi.org/10.3390/nano11051342

117. A. Kypta, H. Blessberger, J. Kammler, M. Lichtenauer, T. Lambert, R. Silye, C. Steinwender, First autopsy description of changes 1 year after implantation of a leadless cardiac pacemaker: Unexpected ingrowth and severe chronic inflammation. Can. J. Cardiol. **32**, 1578.E1–1578.E2 (2016). https://doi.org/10.1016/j.cjca.2015.12.028

118. P. Qi, M.F. Maitz, N. Huang, Surface modification of cardiovascular materials and implants. Surf. Coat. Technol. **233**, 80–90 (2013). https://doi.org/10.1016/j.surfcoat.2013.02.008

119. P. Fosodeder, W. Baumgartner, C. Steinwender, A.W. Hassel, C. Florian, J. Bonse, J. Heitz, Repellent rings at titanium cylinders against overgrowth by fibroblasts. Adv. Opt. Technol. **9**, 113–120 (2020). https://doi.org/10.1515/aot-2019-0070

120. X. Liu, P.K. Chu, C. Ding, Surface modification of titanium, titanium alloys, and related materials for biomedical applications. Mater. Sci. Eng. R Rep. **47**, 49–121 (2004). https://doi.org/10.1016/j.mser.2004.11.001

121. V. Dumas, A. Guignandon, L. Vico, C. Mauclair, X. Zapata, M.T. Linossier, W. Bouleftour, J. Granier, S. Peyroche, J.C. Dumas, H. Zahouani, A. Rattner, Femtosecond laser nano/micro patterning of titanium influences mesenchymal stem cell adhesion and commitment. Biomed. Mater. **10**, 055002 (2015). https://doi.org/10.1088/1748-6041/10/5/055002

122. J.P. Kollender, A.I. Mardare, A.W. Hassel, Direct observation of metal dissolution during anodization of niobium. Electrochem. Commun. **74**, 5–8 (2017). https://doi.org/10.1016/j.elecom.2016.11.011

123. A.I. Mardare, C.D. Grill, I. Pötzelberger, T. Etzelstorfer, J. Stangl, A.W. Hassel, Anodic oxide formation on aluminium-terbium alloys. J. Solid State Electrochem. **20**, 1673–1681 (2016). https://doi.org/10.1007/s10008-016-3139-1

124. K.O. Böker, F. Kleinwort, J.H. Klein-Wiele, P. Simon, K. Jäckle, S. Taheri, W. Lehmann, A.F. Schilling, Laser ablated periodic nanostructures on titanium and steel implants influence adhesion and osteogenic differentiation of mesenchymal stem cells. Materials (Basel). **13**, 3526 (2020). https://doi.org/10.3390/MA13163526

125. M.J. Dalby, N. Gadegaard, R. Tare, A. Andar, M.O. Riehle, P. Herzyk, C.D.W. Wilkinson, R.O.C. Oreffo, The control of human mesenchymal cell differentiation using nanoscale symmetry and disorder. Nat. Mater. **6**, 997–1003 (2007). https://doi.org/10.1038/nmat2013

126. G. Romanos, F. Javed, et al., Peri-implant diseases: A review of treatment interventions. Dent. Clin. N. Am. **59**, 157–178 (2015). https://doi.org/10.1016/j.cden.2014.08.002

127. M.S. Tonetti, Risk factors for osseodisintegration. Periodontol. 2000 **17**, 55–62 (1998). https://doi.org/10.1111/j.1600-0757.1998.tb00123.x

128. S. Ferraris, S. Spriano, Antibacterial titanium surfaces for medical implants. Mater. Sci. Eng. C **61**, 965–978 (2016). https://doi.org/10.1016/j.msec.2015.12.062

129. J. Hasan, H.K. Webb, V.K. Truong, S. Pogodin, V.A. Baulin, G.S. Watson, J.A. Watson, R.J. Crawford, E.P. Ivanova, Selective bactericidal activity of nanopatterned superhydrophobic cicada Psaltoda claripennis wing surfaces. Appl. Microbiol. Biotechnol. **97**, 9257–9262 (2013). https://doi.org/10.1007/s00253-012-4628-5

130. S. Pogodin, J. Hasan, V.A. Baulin, H.K. Webb, V.K. Truong, T.H. Phong Nguyen, V. Boshkovikj, C.J. Fluke, G.S. Watson, J.A. Watson, R.J. Crawford, E.P. Ivanova, Biophysical model of bacterial cell interactions with nanopatterned cicada wing surfaces. Biophys. J. **104**, 835–840 (2013). https://doi.org/10.1016/j.bpj.2012.12.046

131. C.D. Bandara, S. Singh, I.O. Afara, A. Wolff, T. Tesfamichael, K. Ostrikov, A. Oloyede, Bactericidal effects of natural nanotopography of dragonfly wing on Escherichia coli. ACS Appl. Mater. Interfaces **9**, 6746–6760 (2017). https://doi.org/10.1021/acsami.6b13666

132. A. Jaggessar, H. Shahali, A. Mathew, P.K.D.V. Yarlagadda, Bio-mimicking nano and micro-structured surface fabrication for antibacterial properties in medical implants. J. Nanobiotechnol. **15**, 64 (2017). https://doi.org/10.1186/s12951-017-0306-1

133. X. Luo, S. Yao, H. Zhang, M. Cai, W. Liu, R. Pan, C. Chen, X. Wang, L. Wang, M. Zhong, Biocompatible nano-ripples structured surfaces induced by femtosecond laser to rebel bacterial colonization and biofilm formation. Opt. Laser Technol. **124**, 105973 (2020). https://doi.org/10.1016/j.optlastec.2019.105973

134. D. Campoccia, L. Montanaro, C.R. Arciola, A review of the biomaterials technologies for infection-resistant surfaces. Biomaterials **34**, 8533–8554 (2013). https://doi.org/10.1016/j.biomaterials.2013.07.089

135. A. Tripathy, P. Sen, B. Su, W.H. Briscoe, Natural and bioinspired nanostructured bactericidal surfaces. Adv. Colloid Interface Sci. **248**, 85–104 (2017). https://doi.org/10.1016/j.cis.2017.07.030

136. T. Diu, N. Faruqui, T. Sjöström, B. Lamarre, H.F. Jenkinson, B. Su, M.G. Ryadnov, Cicada-inspired cell-instructive nanopatterned arrays. Sci. Rep. **4**, 7122 (2014). https://doi.org/10.1038/srep07122

137. F. Hizal, I. Zhuk, S. Sukhishvili, H.J. Busscher, H.C. Van Der Mei, C.H. Choi, Impact of 3D hierarchical nanostructures on the antibacterial efficacy of a bacteria-triggered self-defensive antibiotic coating. ACS Appl. Mater. Interfaces **7**, 20304–20313 (2015). https://doi.org/10.1021/acsami.5b05947

138. T. Sjöström, A.H. Nobbs, B. Su, Bactericidal nanospike surfaces via thermal oxidation of Ti alloy substrates. Mater. Lett. **167**, 22–26 (2016). https://doi.org/10.1016/j.matlet.2015.12.140

139. A. Mazare, M. Dilea, D. Ionita, I. Titorencu, V. Trusca, E. Vasile, Changing bioperformance of TiO2 amorphous nanotubes as an effect of inducing crystallinity. Bioelectrochemistry **87**, 124–131 (2012). https://doi.org/10.1016/j.bioelechem.2012.01.002

140. X. Fan, B. Feng, Z. Liu, J. Tan, W. Zhi, X. Lu, J. Wang, J. Weng, Fabrication of TiO2 nanotubes on porous titanium scaffold and biocompatibility evaluation in vitro and in vivo. J. Biomed. Mater. Res. – Part A **100**(A), 3422–3427 (2012). https://doi.org/10.1002/jbm.a.34268

141. K. Gulati, S. Ramakrishnan, M.S. Aw, G.J. Atkins, D.M. Findlay, D. Losic, Biocompatible polymer coating of titania nanotube arrays for improved drug elution and osteoblast adhesion. Acta Biomater. **8**, 449–456 (2012). https://doi.org/10.1016/j.actbio.2011.09.004

142. N. Epperlein, F. Menzel, K. Schwibbert, R. Koter, J. Bonse, J. Sameith, J. Krüger, J. Toepel, Influence of femtosecond laser produced nanostructures on biofilm growth on steel. Appl. Surf. Sci. **418**, 420–424 (2017). https://doi.org/10.1016/j.apsusc.2017.02.174

143. K. Schwibbert, F. Menzel, N. Epperlein, J. Bonse, J. Krüger, Bacterial adhesion on femtosecond laser-modified polyethylene. Materials (Basel) **12**, 3107 (2019). https://doi.org/10.3390/ma12193107

144. K. Doll, E. Fadeeva, J. Schaeske, T. Ehmke, A. Winkel, A. Heisterkamp, B.N. Chichkov, M. Stiesch, N.S. Stumpp, Development of laser-structured liquid-infused titanium with strong biofilm-repellent properties. ACS Appl. Mater. Interfaces **9**, 9359–9368 (2017). https://doi.org/10.1021/acsami.6b16159

145. T.S. Wong, S.H. Kang, S.K.Y. Tang, E.J. Smythe, B.D. Hatton, A. Grinthal, J. Aizenberg, Bioinspired self-repairing slippery surfaces with pressure-stable omniphobicity. Nature **477**, 443–447 (2011). https://doi.org/10.1038/nature10447

146. I.A. Paun, B.S. Calin, C.C. Mustaciosu, E. Tanasa, A. Moldovan, A. Niemczyk, M. Dinescu, Laser direct writing via two-photon polymerization of 3D hierarchical structures with cells-antiadhesive properties. Int. J. Mol. Sci. **22**, 5653 (2021). https://doi.org/10.3390/ijms22115653

147. L. Bourdon, J.C. Maurin, K. Gritsch, A. Brioude, V. Salles, Improvements in resolution of additive manufacturing: Advances in two-photon polymerization and direct-writing electro-spinning techniques. ACS Biomater Sci. Eng. **4**, 3927–3938 (2018). https://doi.org/10.1021/acsbiomaterials.8b00810

148. V. Harinarayana, Y.C. Shin, Two-photon lithography for three-dimensional fabrication in micro / nanoscale regime: A comprehensive review. Opt. Laser Technol. **142**, 107180 (2021). https://doi.org/10.1016/j.optlastec.2021.107180

149. A. Atala, R. Lanza, *Methods of Tissue Engineering* (Gulf Professional Publishing, San Diego, 2002)

150. R. Lanza, R. Langer, J. Vacanti, A. Atala, *Principles of Tissue Engineering* (Academic Press, London, 2020)

151. R. Birla, *Introduction to Tissue Engineering: Applications and Challenges* (John Wiley & Sons, Hoboken, 2014)

152. J. Song, C. Michas, C.S. Chen, A.E. White, M.W. Grinstaff, From simple to architecturally complex hydrogel scaffolds for cell and tissue engineering applications: Opportunities presented by two-photon polymerization. Adv. Healthc. Mater. **9**, 1901217 (2020). https://doi.org/10.1002/adhm.201901217

153. C. Frantz, K.M. Stewart, V.M. Weaver, The extracellular matrix at a glance. J. Cell Sci. **123**, 4195–4200 (2010). https://doi.org/10.1242/jcs.023820

154. P. Tayalia, C.R. Mendonca, T. Baldacchini, D.J. Mooney, E. Mazur, 3D cell-migration studies using two-photon engineered polymer scaffolds. Adv. Mater. **20**, 4494–4498 (2008). https://doi.org/10.1002/adma.200801319

155. A. Accardo, M.C. Blatché, R. Courson, I. Loubinoux, C. Vieu, L. Malaquin, Two-photon lithography and microscopy of 3D hydrogel scaffolds for neuronal cell growth. Biomed. Phys. Eng. Express **4**, 027009 (2018). https://doi.org/10.1088/2057-1976/aaab93

156. P. Danilevicius, L. Georgiadi, C.J. Pateman, F. Claeyssens, M. Chatzinikolaidou, M. Farsari, The effect of porosity on cell ingrowth into accurately defined, laser-made, polylactide-based 3D scaffolds. Appl. Surf. Sci. **336**, 2–10 (2015). https://doi.org/10.1016/j.apsusc.2014.06.012

157. R. Schade, T. Weiß, A. Berg, M. Schnabelrauch, K. Liefeith, Two-photon techniques in tissue engineering. Int. J. Artif. Organs **33**, 219–227 (2010). https://doi.org/10.1177/039139881003300406

158. D. Ricci, M.M. Nava, T. Zandrini, G. Cerullo, M.T. Raimondi, R. Osellame, Scaling-up techniques for the nanofabrication of cell culture substrates via two-photon polymerization for industrial-scale expansion of stem cells. Materials (Basel) **10**, 66 (2017). https://doi.org/10.3390/ma10010066

159. A. Trautmann, G.L. Roth, B. Nujiqi, T. Walther, R. Hellmann, Towards a versatile point-of-care system combining femtosecond laser generated microfluidic channels and direct laser written microneedle arrays. Microsyst. Nanoeng. **5**, 6 (2019). https://doi.org/10.1038/s41378-019-0046-5

160. S. Coscoy, S. Baiz, J. Octon, B. Rhoné, L. Perquis, Q. Tseng, F. Amblard, V. Semetey, Micro-topographies control the development of basal protrusions in epithelial sheets. Biointerphases **13**, 041003 (2018). https://doi.org/10.1116/1.5024601

161. I.A. Paun, R.C. Popescu, C.C. Mustaciosu, M. Zamfirescu, B.S. Calin, M. Mihailescu, M. Dinescu, A. Popescu, D. Chioibasu, M. Soproniy, C.R. Luculescu, Laser-direct writing by two-photon polymerization of 3D honeycomb-like structures for bone regeneration. Biofabrication **10**, 025009 (2018). https://doi.org/10.1088/1758-5090/aaa718

162. T. Limongi, L. Brigo, L. Tirinato, F. Pagliari, A. Gandin, P. Contessotto, A. Giugni, G. Brusatin, Three-dimensionally two-photon lithography realized vascular grafts. Biomed. Mater. **16**, 035013 (2021). https://doi.org/10.1088/1748-605X/abca4b

163. A. Koroleva, A. Deiwick, A. Nguyen, S. Schlie-Wolter, R. Narayan, P. Timashev, V. Popov, V. Bagratashvili, B. Chichkov, Osteogenic differentiation of human mesenchymal stem cells in 3-D Zr-Si organic-inorganic scaffolds produced by two-photon polymerization technique. PLoS One **10**, 0118164 (2015). https://doi.org/10.1371/journal.pone.0118164

164. P.S. Timashev, M.V. Vedunova, D. Guseva, E. Ponimaskin, A. Deiwick, T.A. Mishchenko, E.V. Mitroshina, A.V. Koroleva, A.S. Pimashkin, I.V. Mukhina, V.Y. Panchenko, B.N. Chichkov, V.N. Bagratashvili, 3D in vitro platform produced by two-photon polymerization for the analysis of neural network formation and function. Biomed. Phys. Eng. Express **2**, 035001 (2016). https://doi.org/10.1088/2057-1976/2/3/035001

165. K.S. Worthington, L.A. Wiley, E.E. Kaalberg, M.M. Collins, R.F. Mullins, E.M. Stone, B.A. Tucker, Two-photon polymerization for production of human iPSC-derived retinal cell grafts. Acta Biomater. **55**, 385–395 (2017). https://doi.org/10.1016/j.actbio.2017.03.039

166. P.S. Timashev, D. Kuznetsova, A.V. Koroleva, N. Prodanets, A. Deiwick, Y. Piskun, K. Bardakova, N. Dzhoyashvili, S. Kostjuk, E. Zagaynova, Y. Rochev, B. Chichkov, V. Bragatashvili, Novel biodegradable star-shaped polylactide scaffolds for bone regeneration fabricated by two-photon polymerization. Nanomedicine **11**, 1041–1053 (2016). https://doi.org/10.2217/nnm-2015-0022

167. A. Trautmann, M. Rüth, H.D. Lemke, T. Walther, R. Hellmann, Two-photon polymerization based large scaffolds for adhesion and proliferation studies of human primary fibroblasts. Opt. Laser Technol. **106**, 474–480 (2018). https://doi.org/10.1016/j.optlastec.2018.05.008

168. T. Wloka, S. Czich, M. Kleinsteuber, E. Moek, C. Weber, M. Gottschaldt, K. Liefeith, U.S. Schubert, Microfabrication of 3D-hydrogels via two-photon polymerization of poly(2-ethyl-2-oxazoline) diacrylates. Eur. Polym. J. **122**, 109295 (2020). https://doi.org/10.1016/j.eurpolymj.2019.109295

169. S. Engelhardt, E. Hoch, K. Borchers, W. Meyer, H. Krüger, G.E.M. Tovar, A. Gillner, Fabrication of 2D protein microstructures and 3D polymer-protein hybrid microstructures by two-photon polymerization. Biofabrication **3**, 025003 (2011). https://doi.org/10.1088/1758-5082/3/2/025003

170. T. Weiß, R. Schade, T. Laube, A. Berg, G. Hildebrand, R. Wyrwa, M. Schnabelrauch, K. Liefeith, Two-photon polymerization of biocompatible photopolymers for microstructured 3D biointerfaces. Adv. Eng. Mater. **13**, 264–273 (2011). https://doi.org/10.1002/adem.201080090

171. A.K. Nguyen, S.D. Gittard, A. Koroleva, S. Schlie, A. Gaidukeviciute, B.N. Chichkov, R.J. Narayan, Two-photon polymerization of polyethylene glycol diacrylate scaffolds with riboflavin and triethanolamine used as a water-soluble photoinitiator. Regen. Med. **8**, 725–738 (2013). https://doi.org/10.2217/rme.13.60

172. N.A. Bakhtina, M. Müller, H. Wischnewski, R. Arora, C. Ciaudo, 3D synthetic microstructures fabricated by two-photon polymerization promote homogeneous expression of NANOG and ESRRB in mouse embryonic stem cells. Adv. Mater. Interfaces **8**, 2001964 (2021). https://doi.org/10.1002/admi.202001964

173. J.R. Thompson, K.S. Worthington, B.J. Green, N.K. Mullin, C. Jiao, E.E. Kaalberg, L.A. Wiley, I.C. Han, S.R. Russell, E.H. Sohn, C.A. Guymon, R.F. Mullins, E.M. Stone, B.A. Tucker, Two-photon polymerized poly(caprolactone) retinal cell delivery scaffolds and their systemic and retinal biocompatibility. Acta Biomater. **94**, 204–218 (2019). https://doi.org/10.1016/j.actbio.2019.04.057

174. A. Ovsianikov, B. Chichkov, P. Mente, N.A. Monteiro-Riviere, A. Doraiswamy, R.J. Narayan, Two photon polymerization of polymer-ceramic hybrid materials for transdermal drug delivery. Int. J. Appl. Ceram. Technol. **4**, 22–29 (2007). https://doi.org/10.1111/j.1744-7402.2007.02115.x

175. H. Yu, J. Liu, Y.Y. Zhao, F. Jin, X.Z. Dong, Z.S. Zhao, X.M. Duan, M.L. Zheng, Biocompatible three-dimensional hydrogel cell scaffold fabricated by sodium hyaluronate and chitosan assisted two-photon polymerization. ACS Appl. Bio Mater. **2**, 3077–3083 (2019). https://doi.org/10.1021/acsabm.9b00384

176. B. Buchroithner, D. Hartmann, S. Mayr, Y.J. Oh, D. Sivun, A. Karner, B. Buchegger, T. Griesser, P. Hinterdorfer, T.A. Klar, J. Jacak, 3D multiphoton lithography using biocompatible polymers with specific mechanical properties. Nanoscale Adv. **2**, 2422–2428 (2020). https://doi.org/10.1039/d0na00154f

177. J. Heitz, C. Plamadeala, M. Wiesbauer, P. Freudenthaler, R. Wollhofen, J. Jacak, T.A. Klar, B. Magnus, D. Köstner, A. Weth, W. Baumgartner, R. Marksteiner, Bone-forming cells with pronounced spread into the third dimension in polymer scaffolds fabricated by two-photon polymerization. J. Biomed. Mater. Res. – Part A **105**, 891–899 (2017). https://doi.org/10.1002/jbm.a.35959

178. A. Schober, U. Fernekorn, S. Singh, G. Schlingloff, M. Gebinoga, J. Hampl, A. Williamson, Mimicking the biological world: Methods for the 3D structuring of artificial cellular environments. Eng. Life Sci. **13**, 352–367 (2013). https://doi.org/10.1002/elsc.201200088

179. M. Chatzinikolaidou, S. Rekstyte, P. Danilevicius, C. Pontikoglou, H. Papadaki, M. Farsari, M. Vamvakaki, Adhesion and growth of human bone marrow mesenchymal stem cells on precise-geometry 3D organic-inorganic composite scaffolds for bone repair. Mater. Sci. Eng. C **48**, 301–309 (2015). https://doi.org/10.1016/j.msec.2014.12.007

180. F. Klein, B. Richter, T. Striebel, C.M. Franz, G. Von Freymann, M. Wegener, M. Bastmeyer, Two-component polymer scaffolds for controlled three-dimensional cell culture. Adv. Mater. **23**, 1341–1345 (2011). https://doi.org/10.1002/adma.201004060

181. J.K. Hohmann, G. Von Freymann, Influence of direct laser written 3D topographies on proliferation and differentiation of osteoblast-like cells: Towards improved implant surfaces. Adv. Funct. Mater. **24**, 6573–6580 (2014). https://doi.org/10.1002/adfm.201401390

182. R. Nagarkar, M. Singh, H.X. Nguyen, S. Jonnalagadda, A review of recent advances in microneedle technology for transdermal drug delivery. J. Drug Deliv. Sci. Technol. **59**, 101923 (2020). https://doi.org/10.1016/j.jddst.2020.101923

183. E. Larrañeta, M.T.C. McCrudden, A.J. Courtenay, R.F. Donnelly, Microneedles: A new frontier in nanomedicine delivery. Pharm. Res. **33**, 1055–1073 (2016). https://doi.org/10.1007/s11095-016-1885-5

184. A.M. Römgens, D.L. Bader, J.A. Bouwstra, F.P.T. Baaijens, C.W.J. Oomens, Monitoring the penetration process of single microneedles with varying tip diameters. J. Mech. Behav. Biomed. Mater. **40**, 397–405 (2014). https://doi.org/10.1016/j.jmbbm.2014.09.015

185. S. Dharadhar, A. Majumdar, S. Dhoble, V. Patravale, Microneedles for transdermal drug delivery: A systematic review. Drug Dev. Ind. Pharm. **45**, 188–201 (2019). https://doi.org/10.1080/03639045.2018.1539497

186. H.R. Jeong, H.S. Lee, I.J. Choi, J.H. Park, Considerations in the use of microneedles: Pain, convenience, anxiety and safety. J. Drug Target. **25**, 29–40 (2017). https://doi.org/10.1080/1061186X.2016.1200589

187. T.K.L. Kiang, S.A. Ranamukhaarachchi, M.H.H. Ensom, Revolutionizing therapeutic drug monitoring with the use of interstitial fluid and microneedles technology. Pharmaceutics **9**, 43 (2017). https://doi.org/10.3390/pharmaceutics9040043

188. J. Jin, V. Reese, R. Coler, D. Carter, M. Rolandi, Chitin microneedles for an easy-to-use tuberculosis skin test. Adv. Healthc. Mater. **3**, 349–353 (2014). https://doi.org/10.1002/adhm.201300185

189. P. Miller, M. Moorman, R. Manginell, C. Ashlee, I. Brener, D. Wheeler, R. Narayan, R. Polsky, Towards an integrated microneedle total analysis chip for protein detection. Electroanalysis **28**, 1305–1310 (2016). https://doi.org/10.1002/elan.201600063

190. V. Sachdeva, A. Banga, Microneedles and their applications. Recent Pat. Drug Deliv. Formul. **5**, 95–132 (2011). https://doi.org/10.2174/187221111795471445

191. T.N. Tarbox, A.B. Watts, Z. Cui, R.O. Williams, An update on coating/manufacturing techniques of microneedles. Drug Deliv. Transl. Res. **8**, 1828–1843 (2018). https://doi.org/10.1007/s13346-017-0466-4

192. A.S. Cordeiro, I.A. Tekko, M.H. Jomaa, L. Vora, E. Mcalister, F. Volpe-zanutto, M. Nethery, P.T. Baine, N. Mitchell, D.W. Mcneill, F. Ryan, Two-photon polymerisation 3D printing of microneedle array templates with versatile designs: Application in the development of polymeric drug delivery systems. Pharm. Res. **37**, 174 (2020). https://doi.org/10.1007/s11095-020-02887-9

193. S.N. Economidou, D. Douroumis, 3D printing as a transformative tool for microneedle systems: Recent advances, manufacturing considerations and market potential. Adv. Drug Deliv. Rev. **173**, 60–69 (2021). https://doi.org/10.1016/j.addr.2021.03.007

194. S.D. Gittard, B. Chen, H. Xu, A. Ovsianikov, B.N. Chichkov, N.A. Monteiro-Riviere, R.J. Narayan, The effects of geometry on skin penetration and failure of polymer microneedles. J. Adhes. Sci. Technol. **27**, 227–243 (2013). https://doi.org/10.1080/01694243.2012.705101

195. C. Liao, W. Anderson, F. Antaw, M. Trau, Two-photon nanolithography of tailored hollow three-dimensional microdevices for biosystems. ACS Omega **4**, 1401–1409 (2019). https://doi.org/10.1021/acsomega.8b03164

196. C. Plamadeala, S.R. Gosain, F. Hischen, B. Buchroithner, S. Puthukodan, J. Jacak, A. Bocchino, D. Whelan, C. O'Mahony, W. Baumgartner, J. Heitz, Bio-inspired microneedle design for efficient drug/vaccine coating. Biomed. Microdevices **22**, 8 (2020). https://doi.org/10.1007/s10544-019-0456-z

197. M. Leone, J. Mönkäre, J.A. Bouwstra, G. Kersten, Dissolving microneedle patches for dermal vaccination. Pharm. Res. **34**, 2223–2240 (2017). https://doi.org/10.1007/s11095-017-2223-2

198. Z.F. Rad, R.E. Nordon, C.J. Anthony, L. Bilston, P.D. Prewett, J.Y. Arns, C.H. Arns, L. Zhang, G.J. Davies, High-fidelity replication of thermoplastic microneedles with open microfluidic channels. Microsyst. Nanoeng. **3**, 17034 (2017). https://doi.org/10.1038/micronano.2017.34

199. P. Griss, G. Stemme, Side-opened out-of-plane microneedles for microfluidic transdermal liquid transfer. J. Microelectromech. Syst. **12**, 296–301 (2003). https://doi.org/10.1109/JMEMS.2003.809959

200. M. Kavaldzhiev, J.E. Perez, Y. Ivanov, A. Bertoncini, C. Liberale, J. Kosel, Biocompatible 3D printed magnetic micro needles. Biomed. Phys. Eng. Express **3**, 025005 (2017). https://doi.org/10.1088/2057-1976/aa5ccb

201. A. Aksit, D.N. Arteaga, M. Arriaga, X. Wang, H. Watanabe, K.E. Kasza, A.K. Lalwani, J.W. Kysar, In-vitro perforation of the round window membrane via direct 3-D printed microneedles. Biomed. Microdevices **20**, 47 (2018). https://doi.org/10.1007/s10544-018-0287-3

202. C. Plamadeala, F. Hischen, R. Friesenecker, R. Wollhofen, J. Jacak, G. Buchberger, E. Heiss, T.A. Klar, W. Baumgartner, J. Heitz, Bioinspired polymer microstructures for directional transport of oily liquids. R. Soc. Open Sci. **4**, 160849 (2017). https://doi.org/10.1098/rsos.160849

203. B. Buchroithner, P. Spurný, S. Mayr, J. Heitz, D. Sivun, J. Jacak, J. Ludwig, An improved transwell design for microelectrode ion-flux measurements. Micromachines **12**, 273 (2021). https://doi.org/10.3390/mi12030273

204. G. Vizsnyiczai, A. Búzás, B. Lakshmanrao Aekbote, T. Fekete, I. Grexa, P. Ormos, L. Kelemen, Multiview microscopy of single cells through microstructure-based indirect optical manipulation. Biomed. Opt. Express **11**, 945 (2020). https://doi.org/10.1364/boe.379233

205. B.L. Aekbote, T. Fekete, J. Jacak, G. Vizsnyiczai, P. Ormos, L. Kelemen, Surface-modified complex SU-8 microstructures for indirect optical manipulation of single cells. Biomed. Opt. Express **7**, 45 (2016). https://doi.org/10.1364/boe.7.000045

206. T.A. Klar, R. Wollhofen, J. Jacak, Sub-Abbe resolution: From STED microscopy to STED lithography. Phys. Scr. **T162** (2014). https://doi.org/10.1088/0031-8949/2014/T162/014049

207. B. Buchegger, A. Tanzer, S. Posch, C. Gabriel, T.A. Klar, J. Jacak, STED lithography in microfluidics for 3D thrombocyte aggregation testing. J. Nanobiotechnol. **19**, 23 (2021). https://doi.org/10.1186/s12951-020-00762-8

208. F. Hischen, G. Buchberger, C. Plamadeala, O. Armbruster, E. Heiss, K. Winands, M. Schwarz, B. Jüttler, J. Heitz, W. Baumgartner, The external scent efferent system of selected European true bugs (Heteroptera): A biomimetic inspiration for passive, unidirectional fluid transport. J. R. Soc. Interface **15**, 20170975 (2018). https://doi.org/10.1098/rsif.2017.0975

209. A.C. Joel, G. Buchberger, P. Comanns, Moisture-harvesting reptiles: A review, in *FSurfaces in Biology III. Biologically-Inspired Systems*, ed. by S. Gorb, E. Gorb, vol. 10, (Springer International Publishing AG, part of Springer Nature, Switzerland, 2017). https://doi.org/10.1007/978-3-319-74144-4_4

210. P. Comanns, Passive water collection with the integument: Mechanisms and their biomimetic potential. J. Exp. Biol. **221** (2018). https://doi.org/10.1242/jeb.153130

211. G. Buchberger, R. Baumgartner, A. Kogler, T. Fritz, S. Bauer, W. Baumgartner, Bio-inspired "fluidic diode" for large-area unidirectional passive water transport even against gravity. Sens. Actuators, A Phys. **283**, 375–385 (2018). https://doi.org/10.1016/j.sna.2018.09.070

212. G. Buchberger, A. Kogler, A. Weth, R. Baumgartner, P. Comanns, S. Bauer, W. Baumgartner, Fluidic diode for passive unidirectional liquid transport bioinspired by the spermathecae of fleas. J. Bionic Eng. **15**, 42–56 (2018). https://doi.org/10.1007/s42235-017-0003-7

213. G. Buchberger, F. Hischen, P. Comanns, R. Baumgartner, A. Kogler, A. Buchsbaum, S. Bauer, W. Baumgartner, Bio-inspired microfluidic devices for passive, directional liquid transport: Model-based adaption for different materials. Procedia Eng. **120**, 106–111 (2015). https://doi.org/10.1016/j.proeng.2015.08.576

214. P. Comanns, G. Buchberger, A. Buchsbaum, R. Baumgartner, A. Kogler, S. Bauer, W. Baumgartner, Directional, passive liquid transport: The Texas horned lizard as a model for a biomimetic 'liquid diode'. J. R. Soc. Interface **12**, 20150415 (2015). https://doi.org/10.1098/rsif.2015.0415

215. S.V. Kirner, U. Hermens, A. Mimidis, E. Skoulas, C. Florian, F. Hischen, C. Plamadeala, W. Baumgartner, K. Winands, H. Mescheder, J. Krüger, J. Solis, J. Siegel, E. Stratakis, J. Bonse, Mimicking bug-like surface structures and their fluid transport produced by ultrashort laser pulse irradiation of steel. Appl. Phys. A Mater. Sci. Process. **123**, 754 (2017). https://doi.org/10.1007/s00339-017-1317-3

216. M. Erzina, A. Trelin, O. Guselnikova, B. Dvorankova, K. Strnadova, A. Perminova, P. Ulbrich, D. Mares, V. Jerabek, R. Elashnikov, V. Svorcik, O. Lyutakov, Precise cancer detection via the combination of functionalized SERS surfaces and convolutional neural network with independent inputs. Sens. Actuators B **308**, 127660 (2020). https://doi.org/10.1016/j.snb.2020.127660

217. O. Guselnikova, A. Trelin, A. Skvortsova, P. Ulbrich, P. Postnikov, A. Pershina, D. Sykora, V. Svorcik, O. Lyutakov, Label-free surface-enhanced Raman spectroscopy with artificial neural network technique for recognition photoinduced DNA damage. Biosens. Bioelectron. **145**, 111718 (2019). https://doi.org/10.1016/j.bios.2019.111718

218. B. Shan, Y. Pu, Y. Chen, M. Liao, M. Li, Novel SERS labels: Rational design, functional integration and biomedical applications. Coord. Chem. Rev. **371**, 11–37 (2018). https://doi.org/10.1016/j.ccr.2018.05.007

219. I. Bruzas, W. Lum, Z. Gorunmez, L. Sagle, Advances in surface-enhanced Raman spectroscopy (SERS) substrates for lipid and protein characterization: Sensing and beyond. Analyst **143**, 3990–4008 (2018). https://doi.org/10.1039/c8an00606g

220. J. Siegel, P. Slepička, J. Heitz, Z. Kolská, P. Sajdl, V. Švorčík, Gold nano-wires and nano-layers at laser-induced nano-ripples on PET. Appl. Surf. Sci. **256**, 2205–2209 (2010). https://doi.org/10.1016/j.apsusc.2009.09.074

221. L. Kelemen, E. Lepera, B. Horváth, P. Ormos, R. Osellame, R. Martínez Vázquez, Direct writing of optical microresonators in a lab-on-a-chip for label-free biosensing. Lab Chip **19**, 1985–1990 (2019). https://doi.org/10.1039/c9lc00174c

222. E. Koch, A. Dietzel, Stretchable sensor array for respiratory monitoring, in *19th Int. Conf. Solid-State Sensors, Actuators Microsystems (TRANSDUCERS)*, (IEEE, 2017), pp. 2227–2230. https://doi.org/10.1109/TRANSDUCERS.2017.7994520

223. S. Vucinic, B. Antonijevic, A.M. Tsatsakis, L. Vassilopoulou, A.O. Docea, A.E. Nosyrev, B.N. Izotov, H. Thiermann, N. Drakoulis, D. Brkic, Environmental exposure to organophosphorus nerve agents. Environ. Toxicol. Pharmacol. **56**, 163–171 (2017). https://doi.org/10.1016/j.etap.2017.09.004

224. R.K. Ibrahim, M. Hayyan, M.A. AlSaadi, A. Hayyan, S. Ibrahim, Environmental application of nanotechnology: Air, soil, and water. Environ. Sci. Pollut. Res. **23**, 13754–13788 (2016). https://doi.org/10.1007/s11356-016-6457-z

225. M. Benetti, D. Cannatà, E. Verona, A. Palla Papavlu, V.C. Dinca, T. Lippert, M. Dinescu, F. Di Pietrantonio, Highly selective surface acoustic wave e-nose implemented by laser direct writing. Sens. Actuators B **283**, 154–162 (2019). https://doi.org/10.1016/j.snb.2018.12.005

226. B. Steinhauser, C. Vidal, R.A. Barb, J. Heitz, A.I. Mardare, A.W. Hassel, C. Hrelescu, T.A. Klar, Localized-plasmon voltammetry to detect pH dependent gold oxidation. J. Phys. Chem. C **122**, 4565–4571 (2018). https://doi.org/10.1021/acs.jpcc.7b11355

227. E. Koch, A. Dietzel, Respiratory trigger signal generation by means of a stretchable sensor array. Sens. Actuators A Phys. **273**, 113–120 (2018). https://doi.org/10.1016/j.sna.2018.02.022

228. R. Delmdahl, A. Wiessner, Pulsed laser deposition for coating applications. J. Phys. Conf. Ser. **59**, 28–31 (2007). https://doi.org/10.1088/1742-6596/59/1/006

229. M.J. Aziz, Film growth mechanisms in pulsed laser deposition. Appl. Phys. A Mater. Sci. Process. **93**, 579–587 (2008). https://doi.org/10.1007/s00339-008-4696-7

230. T. Yamaguchi, H. Hagino, M. Takemura, Y. Hasegawa, Y. Michiyama, A. Nakahira, Microstructure of FeTiC composite surface layer on carbon steel formed by laser alloying process. Mater. Trans. **54**, 1755–1759 (2013). https://doi.org/10.2320/matertrans.MAW201304

231. A. Milionis, D. Fragouli, I.S. Bayer, A. Athanassiou, Water adhesion to laser-treated surfaces, in *Laser Surface Modification and Adhesion*, (John Wiley & Sons, Hoboken, 2014), pp. 377–413

232. T. Kokubo, H.M. Kim, M. Kawashita, Novel bioactive materials with different mechanical properties. Biomaterials **24**, 2161–2175 (2003). https://doi.org/10.1016/S0142-9612(03)00044-9

233. M. Mozafari, Bioceramics in the realm of history. Bioceram. Dev. Appl. **4**, e106 (2014). https://doi.org/10.4172/2090-5025.1000e106

234. T. Zhai, X. Fang, M. Liao, X. Xu, H. Zeng, B. Yoshio, D. Golberg, A comprehensive review of one-dimensional metal-oxide nanostructure photodetectors. Sensors **9**, 6504–6529 (2009). https://doi.org/10.3390/s90806504

235. M. Azami, S. Jalilifiroozinezhad, M. Mozafari, M. Rabiee, Synthesis and solubility of calcium fluoride/hydroxy-fluorapatite nanocrystals for dental applications. Ceram. Int. **37**, 2007–2014 (2011). https://doi.org/10.1016/j.ceramint.2011.02.025

236. S. Kargozar, N. Lotfibakhshaiesh, J. Ai, M. Mozafari, P. Brouki Milan, S. Hamzehlou, M. Barati, F. Baino, R.G. Hill, M.T. Joghataei, Strontium- and cobalt-substituted bioactive glasses seeded with human umbilical cord perivascular cells to promote bone regeneration via enhanced osteogenic and angiogenic activities. Acta Biomater. **58**, 502–514 (2017). https://doi.org/10.1016/j.actbio.2017.06.021

237. R. Kamalian, A. Yazdanpanah, F. Moztarzadeh, R. Ravarian, Z. Moztarzadeh, M. Tahmasbi, M. Mozafari, Synthesis and characterization of bioactive glass/forsterite nanocomposites for bone and dental implants. Ceram. – Silik. **56**, 331–340 (2012)

238. M. Mozafari, E. Salahinejad, V. Shabafrooz, M. Yazdimamaghani, D. Vashaee, L. Tayebi, Multilayer bioactive glass/zirconium titanate thin films in bone tissue engineering and regenerative dentistry. Int. J. Nanomedicine **8**, 1665–1672 (2013). https://doi.org/10.2147/IJN.S42659

239. L. Torrisi, S. Trusso, G. Di Marco, P. Parisi, Pulsed laser deposition of hydroxyapatite films by KrF excimer. Phys. Med. **17**, 227–231 (2001)

240. C. Capuccini, F. Sima, E. Axente, E. Boanini, M. Gazzano, A. Bigi, I.N. Mihailescu, Strontium-substituted hydroxyapatite thin films grown by pulsed laser deposition, in *Functionalized Nanoscale Materials, Devices and Systems*, (Springer, Dordrecht, 2008), pp. 389–398

241. E.L. Solla, J.P. Borrajo, P. González, J. Serra, S. Chiussi, C. Serra, B. León, M. Pérez-Amor, Pulsed laser deposition of silicon-substituted hydroxyapatite coatings. Vacuum **82**, 1383–1385 (2008). https://doi.org/10.1016/j.vacuum.2008.03.020

242. L. Floroian, B. Savu, G. Stanciu, A.C. Popescu, F. Sima, I.N. Mihailescu, R. Mustata, L.E. Sima, S.M. Petrescu, D. Tanaskovic, D. Janackovic, Nanostructured bioglass thin films synthesized by pulsed laser deposition: CSLM, FTIR investigations and in vitro biotests. Appl. Surf. Sci. **255**, 3056–3062 (2008). https://doi.org/10.1016/j.apsusc.2008.08.105

243. L. Floroian, M. Florescu, F. Sima, G. Popescu-Pelin, C. Ristoscu, I.N. Mihailescu, Synthesis of biomaterial thin films by pulsed laser technologies: Electrochemical evaluation of bioactive glass-based nanocomposite coatings for biomedical applications. Mater. Sci. Eng. C **32**, 1152–1157 (2012). https://doi.org/10.1016/j.msec.2012.03.001

244. C. Piconi, G. Maccauro, Zirconia as a ceramic biomaterial. Biomaterials **20**, 1–25 (1999). https://doi.org/10.1016/S0142-9612(98)00010-6

245. Z. Pang, A. Chughtai, I. Sailer, Y. Zhang, A fractographic study of clinically retrieved zirconia-ceramic and metal-ceramic fixed dental prostheses. Dent. Mater. **31**, 1198–1206 (2015). https://doi.org/10.1016/j.dental.2015.07.003

246. Z. Zhang, M. Guazzato, T. Sornsuwan, S.S. Scherrer, C. Rungsiyakull, W. Li, M.V. Swain, Q. Li, Thermally induced fracture for core-veneered dental ceramic structures. Acta Biomater. **9**, 8394–8402 (2013). https://doi.org/10.1016/j.actbio.2013.05.009

247. C. Sax, 10-year clinical outcomes of fixed dental prostheses with zirconia frameworks. Int. J. Comput. Dent. **14**(3), 183–202 (2011)

248. M.N. Aboushelib, C.J. Kleverlaan, A.J. Feilzer, Microtensile bond strength of different components of core veneered all-ceramic restorations. Part II: Zirconia veneering ceramics. Dent. Mater. **22**, 857–863 (2006). https://doi.org/10.1016/j.dental.2005.11.014

249. N. De Jager, P. Pallav, A.J. Feilzer, The influence of design parameters on the FEA-determined stress distribution in CAD-CAM produced all-ceramic dental crowns. Dent. Mater. **21**, 242–251 (2005). https://doi.org/10.1016/j.dental.2004.03.013

250. M. Dündar, M. Özcan, B. Gökçe, E. Çömlekoğlu, F. Leite, L.F. Valandro, Comparison of two bond strength testing methodologies for bilayered all-ceramics. Dent. Mater. **23**, 630–636 (2007). https://doi.org/10.1016/j.dental.2006.05.004

251. R.L.P. Santos, F.S. Silva, R.M. Nascimento, J.C.M. Souza, F.V. Motta, O. Carvalho, B. Henriques, Shear bond strength of veneering porcelain to zirconia: Effect of surface treatment by CNC-milling and composite layer deposition on zirconia. J. Mech. Behav. Biomed. Mater. **60**, 547–556 (2016). https://doi.org/10.1016/j.jmbbm.2016.03.015

252. Ç. Ural, T. Külünk, Ş. Külünk, M. Kurt, The effect of laser treatment on bonding between zirconia ceramic surface and resin cement. Acta Odontol. Scand. **68**, 354–359 (2010). https://doi.org/10.3109/00016357.2010.514720

253. D. Liu, J.P. Matinlinna, J.K.H. Tsoi, E.H.N. Pow, T. Miyazaki, Y. Shibata, C.W. Kan, A new modified laser pretreatment for porcelain zirconia bonding. Dent. Mater. **29**, 559–565 (2013). https://doi.org/10.1016/j.dental.2013.03.002

254. H.J. Kim, H.P. Lim, Y.J. Park, M.S. Vang, Effect of zirconia surface treatments on the shear bond strength of veneering ceramic. J. Prosthet. Dent. **105**, 315–322 (2011). https://doi.org/10.1016/S0022-3913(11)60060-7

255. B. Henriques, D. Fabris, J.C.M. Souza, F.S. Silva, Ó. Carvalho, M.C. Fredel, J. Mesquita-Guimarães, Bond strength enhancement of zirconia-porcelain interfaces via Nd:YAG laser surface structuring. J. Mech. Behav. Biomed. Mater. **81**, 161–167 (2018). https://doi.org/10.1016/j.jmbbm.2018.02.031

256. F. Chang, T. Liang, T. Wu, C. Wu, Using 3D printing and femtosecond laser micromachining to fabricate biodegradable peripheral vascular stents with high structural uniformity and dimensional precision. Int. J. Adv. Manuf. Technol. **116**, 1523–1536 (2021). https://doi.org/10.1007/s00170-021-07446-z

257. M.H. Smith, C.L. Flanagan, J.M. Kemppainen, J.A. Sack, H. Chung, S. Das, S.J. Hollister, S.E. Feinberg, Computed tomography-based tissue-engineered scaffolds in craniomaxillofacial surgery. Int. J. Med. Robot. Comput. Assist. Surg. **3**, 206–217 (2007). https://doi.org/10.1002/rcs.143

258. F.G. Mangano, B. Cirotti, R.L. Sammons, C. Mangano, Custom-made, root-analogue direct laser metal forming implant: A case report. Lasers Med. Sci. **27**, 1241–1245 (2012). https://doi.org/10.1007/s10103-012-1134-z

259. F. Mangano, M. Bazzoli, L. Tettamanti, D. Farronato, M. Maineri, A. Macchi, C. Mangano, Custom-made, selective laser sintering (SLS) blade implants as a non-conventional solution for the prosthetic rehabilitation of extremely atrophied posterior mandible. Lasers Med. Sci. **28**, 1241–1247 (2013). https://doi.org/10.1007/s10103-012-1205-1

260. C. Li, Y. Yang, L. Yang, Z. Shi, Biomimetic anti-adhesive surface microstructures on electro-surgical blade fabricated by long-pulse laser inspired by pangolin scales. Micromachines **10**, 816 (2019). https://doi.org/10.3390/mi10120816

261. F. Fankhauser, S. Kwasniewska, *Lasers in Ophthalmology: Basic, Diagnostic, and Surgical Aspects* (Netherlands Kugler Publ, Hague, 2003)

262. M.A. Gilmour, Lasers in ophthalmology. Vet. Clin. North Am. Small Anim. Pract. **32**, 649–672 (2002). https://doi.org/10.1016/S0195-5616(02)00009-8

263. H.A. Wigdor, J.T. Walsh, J.D.B. Featherstone, S.R. Visuri, D. Fried, J.L. Waldvogel, Lasers in dentistry. Lasers Surg. Med. **16**, 103–133 (1995). https://doi.org/10.1002/lsm.1900160202

264. M. Miller, T. Truhe, Lasers in dentistry: An overview. J. Am. Dent. Assoc. **124**, 32–35 (1993). https://doi.org/10.14219/jada.archive.1993.0034

265. C. Fornaini, R. Fekrazad, J. Rocca, E. Merigo, Use of blue and blue-violet lasers in dentistry: A narrative review. J. Lasers Med. Sci. **12**, e31 (2021). https://doi.org/10.34172/jlms.2021.31